



**HAL**  
open science

## Relative geomagnetic paleointensity of the Brunhes Chron and the Matuyama-Brunhes precursor as recorded in sediment core from Wilkes Land Basin (Antarctica)

Patrizia Macrì, Leonardo Sagnotti, Jaume Dinarès-Turell, Andrea Caburlotto

► **To cite this version:**

Patrizia Macrì, Leonardo Sagnotti, Jaume Dinarès-Turell, Andrea Caburlotto. Relative geomagnetic paleointensity of the Brunhes Chron and the Matuyama-Brunhes precursor as recorded in sediment core from Wilkes Land Basin (Antarctica). *Physics of the Earth and Planetary Interiors*, 2010, 179 (1-2), pp.72. 10.1016/j.pepi.2009.12.002 . hal-00616885

**HAL Id: hal-00616885**

**<https://hal.science/hal-00616885>**

Submitted on 25 Aug 2011

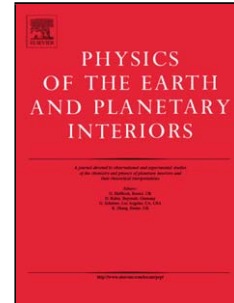
**HAL** is a multi-disciplinary open access archive for the deposit and dissemination of scientific research documents, whether they are published or not. The documents may come from teaching and research institutions in France or abroad, or from public or private research centers.

L'archive ouverte pluridisciplinaire **HAL**, est destinée au dépôt et à la diffusion de documents scientifiques de niveau recherche, publiés ou non, émanant des établissements d'enseignement et de recherche français ou étrangers, des laboratoires publics ou privés.

## Accepted Manuscript

Title: Relative geomagnetic paleointensity of the Brunhes Chron and the Matuyama-Brunhes precursor as recorded in sediment core from Wilkes Land Basin (Antarctica)

Authors: Patrizia Macrì, Leonardo Sagnotti, Jaume Dinarès-Turell, Andrea Caburlotto



PII: S0031-9201(09)00241-6  
DOI: doi:10.1016/j.pepi.2009.12.002  
Reference: PEPI 5230

To appear in: *Physics of the Earth and Planetary Interiors*

Received date: 24-7-2009  
Revised date: 4-12-2009  
Accepted date: 7-12-2009

Please cite this article as: Macrì, P., Sagnotti, L., Dinarès-Turell, J., Caburlotto, A., Relative geomagnetic paleointensity of the Brunhes Chron and the Matuyama-Brunhes precursor as recorded in sediment core from Wilkes Land Basin (Antarctica), *Physics of the Earth and Planetary Interiors* (2008), doi:10.1016/j.pepi.2009.12.002

This is a PDF file of an unedited manuscript that has been accepted for publication. As a service to our customers we are providing this early version of the manuscript. The manuscript will undergo copyediting, typesetting, and review of the resulting proof before it is published in its final form. Please note that during the production process errors may be discovered which could affect the content, and all legal disclaimers that apply to the journal pertain.

1 Relative geomagnetic paleointensity of the Brunhes Chron and the Matuyama-  
2 Brunhes precursor as recorded in sediment core from Wilkes Land Basin  
3 (Antarctica)

4  
5 Patrizia Macri<sup>1</sup>, Leonardo Sagnotti<sup>1</sup>, Jaume Dinarès-Turell<sup>1</sup> and Andrea Caburlotto<sup>2</sup>  
6

7 <sup>1</sup> Istituto Nazionale di Geofisica e Vulcanologia, Via di Vigna Murata 605, 00143 Roma, Italy. (Tel: +39  
8 0651860700; fax: +39 0651860397; e-mail: [macri@ingv.it](mailto:macri@ingv.it)).

9 <sup>2</sup> Istituto Nazionale di Oceanografia e Geofisica Sperimentale, Borgo Grotta Gigante 42/c, 34010  
10 Sgonico, Trieste, Italy  
11

12 **Abstract**

13 Paleomagnetic and rock magnetic investigation was performed on the 35-m long MD03-2595  
14 CADO (Coring Adélie Diatom Oozes) piston core recovered on the continental rise of the  
15 Wilkes Land Basin (East Antarctica). Analysis of the Characteristic Remanent Magnetization  
16 (ChRM) inclination record indicates a normal magnetic polarity for the uppermost 34 m of the  
17 sequence and a distinctive abrupt polarity change at the bottom of the core. This polarity  
18 change, which spans a 27 cm thick stratigraphic interval, represents a detailed record of the  
19 Matuyama-Brunhes (M-B) transition and it is preceded by a sharp oscillation in paleomagnetic  
20 directions that may correlate to the M-B precursor event. Paleomagnetic measurements enable  
21 reconstruction of geomagnetic relative paleointensity (RPI) variations, and a high-resolution age  
22 model was established by correlating the CADO RPI curve to the available global reference RPI  
23 stack, indicating that the studied sequence reaches back to ca 800 ka with an average  
24 sedimentation rate of 4.4 cm/ka. Orbital periodicities (100 ka and 41 ka) were found in the  
25 ChRM inclination record, and a significant coherence of ChRM inclination and RPI record  
26 around 100 ka suggests that long-term geomagnetic secular variation in inclination is controlled  
27 by changes in the relative strength of the geocentric axial dipole and persistent non-dipole  
28 components. Moreover, even if the relatively homogeneous rock magnetic parameters and

29 lithofacies throughout the recovered sequence indicates a substantial stability of the East  
30 Antarctic Ice Sheet during the middle and late Pleistocene, influence of the 100 ka and 41 ka  
31 orbital periodicities has been detected in some rock magnetic parameters, indicating subtle  
32 variations in the concentration and grain-size of the magnetic minerals linked to orbital forcing  
33 of the global climate.

34 **Keywords:** paleomagnetism, relative paleointensity, Brunhes Chron, Matuyama-Brunhes  
35 precursor, Antarctica.

36

## 37 **1. Introduction**

38 Pleistocene sedimentary sequences from peri-Antarctic margins have great potential for studies  
39 of paleoenvironmental changes and past geomagnetic field behavior at high latitudes: the  
40 Antarctic continental rises are very sensitive to past environmental and climatic changes, and  
41 their marine sedimentary sequences may preserve detailed information about past climatic  
42 variations. Well resolved paleomagnetic data from high latitudes are also critically important for  
43 global reconstruction of past geomagnetic field behavior and can provide critical constraints for  
44 geodynamo modelling.

45 The QUASAR (QUaternary Sedimentary processes on the east Antarctic continental Rise)  
46 project of the Italian Programma Nazionale Ricerche in Antartide-PNRA, focus on a multiproxy  
47 analysis of the MD03-2595 CADO (Coring Adélie Diatom Oozes) piston core recovered on the  
48 continental rise of the Wilkes Land Basin (WLB) which consists of a continuous fine-grained  
49 sedimentary sequence with a high chronostratigraphic potential. The QUASAR project aims to  
50 reconstruct sedimentary processes offshore of the east Antarctic continental margin and to infer  
51 climatic fluctuations of the continental East Antarctic Ice Sheet.

52 We present a paleomagnetic and rock magnetic study of the 35-m long CADO core, with the  
53 reconstruction of geomagnetic relative paleointensity (RPI) and Characteristic Remanent  
54 Magnetization (ChRM) direction stratigraphic records. The obtained paleomagnetic data allow

55 to establish of a high-resolution age model and to quantify the sedimentation rate for the  
56 recovered sequence. This is particularly valuable because the corrosive character of Antarctic  
57 deep waters with respect to carbonate implies that peri-Antarctic sediments are commonly  
58 deprived of age constraints derived from micropaleontology or stable isotope stratigraphy.

59 The MD03-2595 CADO core is located just outside the inner core tangent cylinder, an  
60 imaginary cylinder parallel to the Earth's spin axis that circumscribes the equator of the inner  
61 core and intersects the surface of the Earth in the polar regions at a latitude of ca 69.6° in both  
62 hemispheres. Different models indicate that geodynamo action occurs mainly by polar vortices  
63 within the tangent cylinder [e.g., Glatzmaier and Roberts, 1995a; Aurnou et al., 2003] or by  
64 differential rotation outside the tangent cylinder [e.g., Kuang and Bloxham, 1997]. Glatzmaier  
65 and Roberts [1995b] showed that there were strong toroidal fields and differential rotation  
66 within the tangent cylinder, with high density of magnetic flux patches that strengthen the non-  
67 dipolar component of the geomagnetic field over the polar regions. This might cause a larger  
68 dynamics, complexity and variability of the geomagnetic field within the tangent cylinder with  
69 respect to the intermediate and low latitudes. The available paleomagnetic study of several cores  
70 from the Arctic region indicates that the magnetic field has been strongly variable during at least  
71 the last 300 ka [e.g. Nowaczyk and Antonow, 1997; Nowaczyk and Frederichs, 1999], with  
72 geomagnetic excursions more frequent and of longer duration than elsewhere. In this context,  
73 only additional studies on sedimentary sequences from southern and northern high latitudes can  
74 provide the necessary experimental evidence to understand past geomagnetic variability within  
75 the polar regions, inside or close to the surface projection of the tangent cylinder.

76 In this context, since there are only few relative paleointensity determinations from high  
77 southern latitudes, along the peri-Antarctic margins [e.g. Brachfeld et al., 2000; 2003; Sagnotti  
78 et al., 2001; Macrì et al., 2005; 2006], the reconstruction of a high-resolution paleomagnetic  
79 record from the CADO sediments represents a valuable input for understanding geomagnetic  
80 field dynamics in the Antarctic region during the past few kyrs.

81  
82  
83  
84  
85  
86  
87  
88  
89  
90  
91  
92  
93  
94  
95  
96  
97  
98  
99  
100  
101  
102  
103  
104  
105

## **2 Geological setting and lithostratigraphy**

The MD03-2595 CADO core was recovered during the MD130 cruise of the R/V “Marion Dufresne II” from the continental rise of the WLB on a sediment wave field in front of the Mertz Glacier (Lat. 64° 54.04 S, Long. 144° 46.37 E) (Fig. 1A). The depositional system of the WLB was formerly investigated by the joint Australian and Italian WEGA (WilkeS land Glacial history) Project, with about 600 km of multichannel seismic reflection and 3.5 kHz acoustic profiles and 11 piston cores triggered [see Brancolini and Harris, 2000]. The morphology of this area is characterized by several submarine canyons incising the slope, and a ridge-channel system perpendicular to the continental margin that originated from the interplay of turbidites and bottom currents [Escutia et al., 1997; Rebesco et al., 1997; Buseti et al., 2003]. The 35-m long CADO core was collected along the transect “Line W39” (Fig. 1A) crossing the depositional flank of the sediment ridge B and the Buffon Canyon (Fig. 1B), and it recovered a continuous sedimentary sequence characterized by a higher chronostratigraphic potential with respect to the already studied and relatively short WEGA cores (each ca 4 meter long) collected in the adjacent area (see Fig. 1A). The sedimentary sequence consists of very fine-grained terrigenous sediments including intervals of massive homogeneous mud, with some sparse fine-grained ice rafted debris (IRD), alternated to laminated mud intervals interpreted as the result of traction currents and/or distal turbidities [Escutia et al., 1997; Buseti et al., 2003; Caburlotto, 2003]. The massive mud facies appears bioturbated, particularly in the first 6 m at the top of the core, and are characterized by a relatively higher content of organic matter and well preserved open-ocean diatoms. The laminated intervals are composed of mm- to cm-thick muddy and silty layers with lack of bioturbation and general lower content of organic matter.

## **3. Sampling and methods**

106 In December 2004, 1.5 m long u-channels were sampled from the 24 archive sections of the  
107 MD03-2595 core at the core repository of the Antarctic Climate and Ecosystems Cooperative  
108 Research Centre-CRC in Canberra, Australia. Because of empty sections, u-channel samples  
109 were not collected for 640-660 cm, 790-820 cm, 1007-1050 cm, 1209-1221 cm, and 1450-1519  
110 cm depth intervals of core.

111 The u-channels were then measured in a magnetically shielded paleomagnetic laboratory at the  
112 Istituto Nazionale di Geofisica e Vulcanologia, Rome, using an automated pass through 2-G  
113 Enterprises DC SQUID cryogenic magnetometer system with a 4.5 cm pass through diameter  
114 access and an in-line Bartington instrument MS2C susceptibility loop sensor, a set of three  
115 orthogonal alternating field (AF) demagnetizing coils with optional anhysteretic remanent  
116 magnetization (ARM) capabilities and an isothermal remanent magnetization (IRM) pulse  
117 magnetizer. High-resolution (1-cm spacing) records of natural remanent magnetization (NRM),  
118 ARM and low-field volume specific magnetic susceptibility ( $\kappa$ ) were obtained for all u-channels  
119 from the MD03-2595 core.

120 The raw magnetic moment data measured by the three orthogonal SQUID sensors of the  
121 cryogenic magnetometer were corrected, directly by the measuring software, taking into account  
122 the different areas under the SQUID response curves. This correction compensates for the  
123 effects of the negative regions on the edge of the response functions for the transverse axes and  
124 for the broader width of the response function along the long axis of the u-channel. It therefore  
125 ensures that the data are free from artefacts that may result from an inadequate consideration of  
126 the different widths and shapes of the response functions for the three SQUID pick-up coils,  
127 which could result in fictitious inclination shallowing (or steepening) of the paleomagnetic data  
128 [see Roberts, 2006]. Moreover, we took particular care in avoiding artefacts eventually due to  
129 deformation effects introduced during sampling, which could result in remanence deflections.  
130 We adopted a conservative approach in this study, disregarding the paleomagnetic data for  
131 ~5cm at both ends of each u-channel and stratigraphic gap.

132 After measuring  $\kappa$ , the NRM was progressively subjected to alternating field (AF)  
133 demagnetization in nine steps up to a maximum peak field of 100 mT. Then, an ARM was  
134 imparted by translating the u-channels at a speed of 10 cm/s in a constant symmetric AF of 100  
135 mT with a superimposed direct current (DC) bias field of 0.1 mT, which was subsequently  
136 stepwise demagnetized using the same sequence of AF steps applied to the NRM. An IRM was  
137 then imparted in a steady DC field of 0.9 T. However the intensity of the IRM exceeded the  
138 dynamic range of the SQUIDS, so we do not report these data below. In order to investigate the  
139 magnetic mineralogy of the sediments, specific rock magnetic investigations were also  
140 performed on eight representative powder samples. Magnetic susceptibility variations in  
141 heating-cooling cycles from room temperature up to 700°C were obtained using a Kappabridge  
142 KLY-3 AGICO magnetic susceptibility meter, coupled with a CS3 furnace. Hysteresis  
143 properties, including coercive force ( $B_C$ ), saturation remanent magnetization ( $M_{RS}$ ) and  
144 saturation magnetization ( $M_S$ ) were measured on a MicroMag alternating gradient  
145 magnetometer (AGM model 2900, Princeton Measurements Corporation) with a maximum  
146 applied field of 1 T. The acquisition of an IRM, and subsequent back-field remagnetization,  
147 both in a succession of fields up to 1 T, was obtained with the same AGM instrument. The  
148 remanent coercive force ( $B_{CR}$ ) was computed from the back-field remagnetization curves.

149

## 150 **4. Results**

### 151 **4.1. Paleomagnetism**

152 Demagnetization diagrams (Fig. 2) indicate stable paleomagnetic behavior throughout most of  
153 the core, with the data aligned along linear demagnetization paths toward the origin, after  
154 removal of a viscous low coercivity remanence component at 10-20 mT. The characteristic  
155 remanent magnetization (ChRM) was computed by principal component analysis on the  
156 individual linear demagnetization paths [Kirschvink, 1980], measured at 1 cm spacing, and was  
157 generally isolated in the 20-80 mT, or rarely 40-80 mT, step intervals. The ChRM was not



158 identified in a few short intervals, that are characterized by unstable paleomagnetic behavior,  
159 and for the depth interval 1955-2095 cm, because a technical trouble occurred during  
160 demagnetization steps higher than 20mT for u-channel 14. Fig. 3 shows the downcore  
161 stratigraphic trends of the ChRM declination and inclination, the maximum angular deviation  
162 (MAD) and the RPI curves  $NRM_{20mT}/\kappa$  and  $NRM_{20mT}/ARM_{20mT}$ . The high latitude of the study  
163 site guarantees that the ChRM inclination is representative enough of the paleomagnetic vectors,  
164 and can provide unambiguous identification of the paleomagnetic polarity. The ChRM  
165 inclination trend shows that the core is mostly of normal polarity. A distinctive abrupt polarity  
166 change is recorded at the bottom of the core, across ca 27 cm of section, with the  $0^\circ$  inclination  
167 mid-point positioned at a depth of ca 3400 cm. About 45 cm below the polarity transition,  
168 another sharp inclination swing, spanning ca 12 cm of section, is recorded: the inclinations pass  
169 again through the horizontal, approach full normal polarity ( $-73^\circ$ ), and then quickly progress to  
170 shallow values and finally return back to the reverse polarity mean values. With regards to the  
171 ChRM declination, we point out that even if the absolute azimuthal orientation is not granted for  
172 each u-channel and relative azimuthal displacements are possible at each u-channel and  
173 stratigraphic break, it generally consistently oscillates around  $360^\circ$ . A few sharp, and  
174 stratigraphically limited, ChRM declination oscillations mostly correspond to intervals of nearly  
175 vertical ChRM or to the polarity transition. MAD angles are usually less than  $2^\circ$  along the core,  
176 indicating that the ChRM directions are generally very well defined; higher values (MAD up to  
177  $15^\circ$ ) were obtained for a few intervals at the bottom of the core in correspondence to the polarity  
178 transition (Fig. 3). The RPI records, computed by normalizing the  $NRM_{20mT}$  by  $\kappa$  and  $ARM_{20mT}$ ,  
179 show a similar pattern supporting a general coherency between the two normalization  
180 procedures. RPI records will be discussed in closer detail in section 4.3.

181

## 182 **4.2 Rock magnetism**

183 In Fig. 4 we show the downcore stratigraphic trends of the main rock magnetic parameters  
184 measured for the MD03-2595 CADO core. Oscillations of the magnetic susceptibility  $\kappa$  and of  
185 the  $ARM_{0mT}$  intensities throughout the core are limited, with values comprised within the same  
186 order of magnitude, which is one of the requisites to obtain reliable RPI estimates (e.g., Tauxe,  
187 1993). In particular,  $\kappa$  fluctuates around a mean value of  $35 \times 10^{-5}$  SI (with a full range of  
188 variability from ca  $5 \times 10^{-5}$  SI to  $60 \times 10^{-5}$  SI), with few sharp peaks corresponding to sparse  
189 pebbles or mm thick silty layers.  $ARM_{0mT}$  mostly oscillates around  $2 \times 10^{-1}$  A/m (with a full  
190 range of variability from 0.05 to  $5 \times 10^{-1}$  A/m). As a result of the limited variation of both  $\kappa$  and  
191  $ARM_{0mT}$ , the  $ARM_{0mT}/\kappa$  ratio is also rather constant, with values fluctuating between 0.5 and  
192  $1.5 \times 10^3$  A/m. The median destructive field of the NRM ( $MDF_{NRM}$ ) is generally comprised  
193 between 10 and 40 mT; several swings to lower and higher  $MDF_{NRM}$  values (from 5 mT to 50  
194 mT, respectively) are evident in the bottom part of the core (last 3-4 m) where the intensity of  
195 the NRM is lower. The  $MDF_{ARM}$  values show a substantial uniformity as well, with a mean  
196 value of ca 28 mT. The ranges of variability for all the rock magnetic parameters are very  
197 similar to the those observed in the nearby WEGA cores [Macri et al., 2005].

198 In order to perform rock magnetic analysis, 8 sub-samples were directly picked from the u-  
199 channels at different selected levels corresponding to high/low  $MDF_{NRM}$  or  $ARM_{0mT}/\kappa$  values  
200 (Fig. 4). All thermomagnetic curves (Fig. 5A, B, C) show an abrupt decrease of the magnetic  
201 susceptibility value at a temperature of  $550^{\circ}$ - $580^{\circ}$ C, corresponding to the Curie temperature of  
202 magnetite ( $Fe_3O_4$ ). Several samples are also characterized by a peak at ca  $280^{\circ}$ C followed by a  
203 distinctive decrease between  $280^{\circ}$ C and  $430^{\circ}$ C (fig 5A, B), that may be due to the thermally  
204 induced conversion of maghaemite ( $\gamma$ - $Fe_2O_3$ ) to haematite ( $\alpha$ - $Fe_2O_3$ ) [Stacey and Banerjee,  
205 1974]. The presence of hematite is indicated by the decreasing trend of the heating curves above  
206  $580^{\circ}$ C, which is observed in some samples. A thermally induced production of newly formed  
207 magnetite is indicate by the cooling curves which are always well above the heating curves (e.g.

208 fig 5A). Hysteresis loops from the same samples generally indicate a coercivity ( $B_c$ ) of ca 20  
209 mT (Fig. 6A), only two samples are characterized by lower coercivity ( $B_c$  of ca 10 mT) (Fig.  
210 6B). The hysteresis ratios mostly fall in a restricted region of the “Day plot” [Day et al., 1977],  
211 typical of pseudo-single domain (PSD) magnetite grains (Fig. 6C). The  $\kappa$ ARM vs.  $\kappa$  plot can be  
212 used to infer grain size variations of ferrimagnetic particles [e.g. King et al., 1983], even if we  
213 recognize that, in practice, it cannot be rigorously applied to determine the actual grain size of  
214 magnetite particles because the ARM intensity varies significantly depending on the  
215 experimental procedures, not yet fully standardized between individual laboratory [see Sagnotti  
216 et al., 2003], and because magnetostatic interaction may affect the efficiency of ARM  
217 acquisition [Sugiura, 1979; Yamazaki and Ioka, 1997]. However, the  $\kappa$ ARM vs.  $\kappa$  plot indicates  
218 a substantial uniformity in the overall magnetic mineral grain size of the sediments (Fig. 6D),  
219 with few, but pronounced, departures from the main cluster of the data corresponding to  
220 distinctive peaks in the magnetic susceptibility linked to rare pebbles or silty layers (i.e. 30-33  
221 cm, 1792-1795 cm, 2826-2829 cm, 2934-2937 cm and 3181-3193 cm depth intervals, see Fig.  
222 3). These intervals, which provided rock magnetic data out of the typical range of variability,  
223 were not taken into account for the reconstruction of the RPI records.

224 Further rock magnetic measurements are available on 70 discrete samples selected from the  
225 WEGA cores [see Macri et al., 2005], which show hysteresis parameters and thermomagnetic  
226 curves that are very similar to those measured for the CADO samples.

227 We conclude that all the rock magnetic parameters of the WEGA and the CADO cores indicate  
228 that these sediments share the same magnetic carriers, which consists of low-coercivity  
229 minerals, most likely represented by a mixture of PSD magnetite and maghemite grains.

230

### 231 **4.3 Relative paleointensity and age model**

232 As the CADO core shows a well defined ChRM and fulfils the basic requirements of a  
233 substantial uniformity in lithology and in concentration, composition and grain size of the

234 magnetic minerals [King et al., 1983; Meynadier et al., 1992; Tauxe, 1993; Valet and  
235 Meynadier, 1998], we used the obtained paleomagnetic and rock magnetic data to reconstruct  
236 variation in relative paleointensity of the geomagnetic field. RPI curves were computed by  
237 normalizing the NRM demagnetized at 20 mT with different concentration-dependent rock  
238 magnetic parameters ( $\text{NRM}_{20\text{mT}}/\kappa$  and  $\text{NRM}_{20\text{mT}}/\text{ARM}_{20\text{mT}}$ ) (see Fig. 3). All the data far from  
239 the uniformity criteria, and that could affect the normalized intensities, were not included in the  
240 reconstruction of the RPI records. The two RPI curves generally match closely, showing the  
241 same stratigraphic patterns throughout the core and only different amplitude in some levels.  
242 We considered the  $\text{NRM}_{20\text{mT}}/\kappa$  record as the best RPI proxy (as discussed below) and then we  
243 correlated it to the available global RPI stack SINT-800 of Guyodo & Valet [1999] (Fig. 7A).  
244 Ages from the dated reference curve were transferred to the CADO RPI record on the basis of  
245 visual correlation of the main paleointensity features using the Analyseries 1.2 software of  
246 Paillard et al. [1996], which allows adjustment and dating between selected pairs of depth and  
247 age tie points of two numerical series. Result of correlation indicates that the CADO core  
248 extends back to about 800 ka across the Matuyama-Brunhes (M-B) polarity transition (Fig. 7B).  
249 The reconstructed average sediment accumulation rate ranges from 1.6 to 8.6 cm/ka (as  
250 calculated from the ages assigned at the individual tie-points; see the step-like line in Fig. 7C).  
251 The mean sedimentation rate for the entire core is 4.4 cm/ka, which is compatible with its  
252 position within the WLB, close to the depositional flank of the sediment ridge B. By  
253 comparison, the average sedimentation rates for six short cores collected in an adjacent area  
254 varied between 19 cm/ka for core PC19 along the WEGA channel and 0.6 cm/ka for core PC20  
255 which was recovered from a ridge crest [Macrì et al., 2005].  
256 The CADO RPI record was also compared with the PISO-1500 global RPI stack recently  
257 published by Channell et al. [2009] and with other southern high latitude records compiled by  
258 Tauxe and Yamazaki [2007] and available from the database of the Magnetics Information

259 Consortium (MagIC) website (Fig. 8). This comparison indicates that the major RPI lows may  
260 be considered global in nature and serve as a target for age control.

261 In order to confirm the efficiency of the RPI normalization procedure, we tested whether the  
262 normalized records are coherent with respect to each other and with respect to the normalization  
263 parameters, using the coherence function (Fig. 9). Times series were at first prepared by  
264 removing any linear trend using a linear function (integration method), after that the spectral  
265 analysis was performed using the software package Analyseries 1.2 [Paillard et al., 1996] with  
266 the Blackman-Tukey method, a Bartlett window and a band-width of ca  $0.006 \text{ kyr}^{-1}$ .

267 The coherence function analysis suggests that the normalized intensity curves are coherent with  
268 each other over most of the relevant frequency range, but they are generally not coherent with  
269 the normalization parameters, especially for  $\text{NRM}_{20\text{mT}}/\kappa$  series (showing significant coherence  
270 above the 95% confidence level only in frequencies from 0.005 to 0.011, roughly around the  
271 100 kyr eccentricity cycle) (Fig. 9A). A coherence extending also to higher and lower  
272 frequencies was obtained for the  $\text{NRM}_{20\text{mT}}/\text{ARM}_{20\text{mT}}$  and  $\text{ARM}_{20\text{mT}}$  parameters. Usually the  
273 efficiency of ARM acquisition may be decreased by magnetostatic interaction between SD  
274 grains [Sugiura, 1979]. This effect could bring to an erroneous evaluation of the magnetizability  
275 of the sediment when using ARM as the normalizer for relative paleointensity estimations and  
276 may result in a significant coherence between the  $\text{NRM}/\text{ARM}$  and  $\text{ARM}$  [Yamazaki, 2008].  
277 However, magnetostatic interaction is not likely to produce important effects in the CADO  
278 sediments, which are mostly characterized by PSD ferromagnetic grains. In any case, we  
279 conclude that the magnetic susceptibility  $\kappa$  is the best choice for RPI normalization of the  
280 sampled sequence, although we recognize that a climatic overprint at eccentricity frequency  
281 may affect the reconstructed RPI curve.

282 A significant coherence appears between ChRM inclination variations and paleointensity  
283 ( $\text{NRM}_{20\text{mT}}/\kappa$ ), though no such coherency was observed between ChRM inclination and  
284  $\text{ARM}_{0\text{mT}}/\kappa$  confirming that shallow inclinations are not influenced by magnetic grain size (Fig.

285 9B). As expected, there is some coherency and an in-phase relationship between  $\text{NRM}_{20\text{mT}}/\kappa$   
286 and  $\text{ARM}_{0\text{mT}}/\kappa$  records in specific intervals of the time series, indicating a magnetic grain size  
287 dependency of the RPI record. However, even if the efficiency of the remanence acquisition  
288 seems to be influenced by magnetic grain size, the coherency of the computed  $\text{NRM}_{20\text{mT}}/\kappa$  with  
289 the SINT-800 reference curve of Guyodo and Valet [1999] (Fig. 9B) and with the PISO-1500  
290 stack of Channell et al. [2009] (Fig. 9C), over most of the frequency spectrum indicates that the  
291 reconstructed geomagnetic RPI variations are significant and can be globally correlated. With  
292 the aim to detect the presence of possible periodicities in the time series, standard Fourier  
293 spectra were calculated for normalization parameters ( $\text{ARM}_{20\text{mT}}$  and  $\kappa$ ), the normalized RPI  
294 records ( $\text{NRM}_{20\text{mT}}/\kappa$  and  $\text{NRM}_{20\text{mT}}/\text{ARM}_{20\text{mT}}$ ) and for ChRM inclination and  $\text{ARM}_{0\text{mT}}/\kappa$  ratio  
295 (Fig. 10). Spectral analysis did not point out any periodicity corresponding to the Milankovitch  
296 orbital precession (19-23 ka), obliquity (41 ka) or eccentricity (100 ka) cycles for the  
297 normalized RPI curves ( $\text{NRM}_{20\text{mT}}/\kappa$  and  $\text{NRM}_{20\text{mT}}/\text{ARM}_{20\text{mT}}$ ), but reveals a significant 100 ka  
298 periodicity for both the normalizing parameters  $\kappa$  and  $\text{ARM}_{20\text{mT}}$ , with a minor influence of the  
299 41 ka periodicity for the magnetic susceptibility  $\kappa$ . Orbital eccentricity and obliquity  
300 periodicities also appear in the ChRM inclination and  $\text{ARM}_{0\text{mT}}/\kappa$  parameters.

301

#### 302 **4.4 ChRM inclination, VGP directions and the M-B polarity reversal**

303 Above the reverse to normal polarity transition, the ChRM inclination values fluctuate around a  
304 mean value of ca  $-68^\circ$ , which is ca  $8^\circ$  shallower than the geomagnetic inclination value of  $-76.8^\circ$   
305 expected at the high latitude of the coring site (Fig. 11). Paleomagnetic inclination shallowing is  
306 a well known process linked to deposition of magnetic particles and subsequent sediment  
307 compaction [Deamer and Kodama 1990; Arason and Levi, 1990]. Shallow bias, or inclination  
308 error, has been found in laboratory re-deposition experiments and in some modern natural  
309 sediments [see Tauxe and Kent, 1984; 2004; Tan et al., 2003]. The inclination shallowing

310 observed in sediments deposited in saline waters could also be a function of the process of  
311 flocculation, which in turn relates to clay content [van Vreumingen, 1993a;b]. A recent  
312 numerical modelling of the relationship between inclination shallowing and relative  
313 paleointensity in sediments indicates that in absence of inclination shallowing the relative  
314 paleointensity recording mechanism may be non-linear [Mitra and Tauxe, 2009]. The  
315 occurrence of inclination shallowing appears therefore as a prerequisite for reliable relative  
316 paleointensity studies. However, the CADO ChRM inclination record in the interval of constant  
317 normal polarity shows some short-lived swings to anomalously low values (i.e.  $<45^\circ$  see Fig. 3),  
318 that cannot be justified by a sedimentary inclination shallowing only. The frequency of  
319 anomalously shallow ChRM inclination data (see histogram of Fig. 11A) is similar to that found  
320 on Antarctic lava flows of the Erebus volcanic province [Lawrence et al, 2009], which supports  
321 the geomagnetic origin of these features. In the following, we will try to verify if, according to  
322 the RPI age model, such shallow ChRM inclinations in the CADO core may correlate to age of  
323 known global geomagnetic excursions of the Brunhes Chron [for comprehensive reviews see  
324 Langereis et al., 1997; Lund et al., 1998; Singer et al., 2002; Channell, 2006; Thouveny et al.,  
325 2004; 2008; Roberts, 2008].

326 In Fig. 12 the ChRM inclination and the virtual geomagnetic poles (VGP) latitude of the CADO  
327 core are plotted versus age and compared to the CADO RPI and the SINT-800 RPI stack, with  
328 vertical grey bars drawn to indicate the main intervals of low RPI in the SINT-800 stack of  
329 Guyodo and Valet [1999]. The position of the main established geomagnetic excursions for the  
330 Brunhes Chron is indicated by arrows, with their estimated age range mostly derived from the  
331 Geomagnetic Instability Time Scale (GITS) of Singer et al. [2002; 2008], and the review of  
332 Thouveny et al. [2008]. The validated geomagnetic excursions, *sensu* Roberts [2008], are  
333 indicated in bold.

334 Starting from the younger RPI minimum, we observe that a long interval of shallow inclination  
335 (up to ca  $-30^\circ$ ) occurs around 20-35 ka ( $MAD < 1^\circ$ ). This age range includes the occurrence of

336 the Mono Lake excursion whose age has been established at 32 ka by Singer et al. [2008].  
337 According to our reconstructed age model, a data gap occurs around 41 ka, the age of the  
338 Laschamp excursion [Guillou et al. 2004]. Lower in the sequence, a distinct sharp shallow  
339 inclination peak (up to  $-42^\circ$ ), corresponding to a broad RPI minimum, occurs at 108 ka, close  
340 the age interval assigned to the Blake excursion (ca 110-120 ka, Tric et al. [1991]; Zhu et al.  
341 [1994]). All the mentioned shallow ChRM inclination values correspond to intervals with  
342 average ARM/ $\kappa$  and  $MDF_{NRM}$  values, and are characterized by well defined ChRM with  
343  $MAD < 2^\circ$ , therefore they do not seem to represent zones of local unusual magnetic mineralogy.  
344 On the contrary, other oscillations to anomalously shallow ChRM values (up to ca  $-35^\circ$   
345  $MAD < 1.5^\circ$ ), observed at ca 62 ka, 279 ka and 404 ka, that do not correlate to any of the  
346 established Brunhes geomagnetic excursions, correspond to a bioturbated layer with darker  
347 mottles, a silty layer and a layer with sparse pebbles, respectively.

348 Several smoothing processes affect the ability of a sedimentary sequence to record transient  
349 geomagnetic features, including smoothing of the geomagnetic signal due to lock-in processes  
350 or magnetic mineral reduction related to diagenesis [i.e., deMenocal et al. 1990; Lund and  
351 Keigwin, 1994; Tarduno and Wilkison, 1996; Roberts and Winklhofer, 2004; Sagnotti et al.,  
352 2005], or due to the instrumental response function of the pick-up coils in the magnetometer  
353 [Oda and Shibuya, 1996; Guyodo et al., 2002]. In the CADO core the absence of clear records  
354 of many known geomagnetic excursions may probably results from smoothing associated to the  
355 relatively low sedimentation rate (on average ca 4.4 cm/kyr) that could be unsuitable to preserve  
356 the details of transient geomagnetic field variations [see Lund and Keigwin, 1994; Kent and  
357 Schneider, 1995; Roberts and Winklhofer, 2004; Roberts, 2008]. An alternative explanation is  
358 that geomagnetic excursions were not globally manifested and they did not produce large  
359 deviations from the average geomagnetic field directions at the location of the CADO core. In  
360 fact, there is a counter argument in the literature against the significance of post-depositional  
361 sedimentary smoothing [e.g. Tauxe et al., 1996; Tauxe, 2006], which supports the hypothesis



362 that the sediment magnetization is locked within the top few centimeters (see the comprehensive  
363 review paper by Tauxe and Yamazaki, 2007).

364 Fig. 13 shows the ChRM inclination, declination, MAD and VGP computed for the bottom (last  
365 100 ka) of the core. The polarity reversal recorded at ca 780 ka can be correlated to the  
366 Matuyama-Brunhes (M-B) transition (whose mid-point was dated at ca 789 ka by Quidelleur et  
367 al. [2003], at ca 774 ka by Channell et al. [2004], at ca 776 ka by Coe et al. [2004] and Singer et  
368 al. [2008]). The M-B transition feature is defined by a reverse- to normal polarity change, taking  
369 place within a 27 cm interval, which occurs in a single u-channel and correlates to a RPI  
370 minimum [see Kent and Schneider, 1995; Channell et al., 2004]. Taking into account the  
371 average sedimentation rate of 4.4 cm/ka calculated by the RPI correlation for this interval, the  
372 time it takes for the full directional change corresponds to 6.8 ka, which is comparable to the  
373 duration for the M-B reversal proposed in the literature [Tauxe et al., 1996; Coe et al., 2004;  
374 Clement 2004; Hyodo et al., 2006].

375 Below the transition, at ca 790 ka, an abrupt inclination swing, reaching values of the full  
376 normal polarity mean ( $-74^\circ$ ), could be correlated to a globally recognized precursor of the M-B  
377 reversal which has been previously reported in deep-sea cores from different oceans and dated  
378 from 10 to 17 ka prior to the M-B reversal, with a duration estimated from 2 to 5 ka [Kent and  
379 Schneider, 1995; Hartl and Tauxe, 1996; Yamazaki and Oda, 2001, Dinarès-Turell et al., 2002].

380 The precursor was also radiometrically dated in various volcanic sites with an age range  
381 spanning from ca 791-793 to 798 ka [Singer et al., 2002; Coe et al., 2004; Brown et al., 2004].

382 Considering again a mean sedimentation rate of 4.4 cm/ka for this part of the MD03-2595  
383 CADO core, the duration of the precursor (spanning ca 12 cm of stratigraphic interval) should  
384 be ca 2.7 ka, with a time interval between the mid-point of the reversal and the precursor of ca  
385 10 ka. Both are estimates in good agreement with the values reported in the literature [see  
386 Channell et al., 2004; Hyodo et al., 2006].

387 In principle, a delayed lock-in of the remanent natural magnetization in the stratigraphic  
388 intervals slightly older than a geomagnetic reversal may cause a record of apparent multiple  
389 polarity changes of the ChRM component in a sedimentary sequence [see Spassov et al., 2003].  
390 This process is caused by variable relative contributions of quite different remanence carriers  
391 and components during the reversal, and could give rise to an irregular polarity lock-in at  
392 different stratigraphic depths. In the CADO core, however, the homogeneity of the lithology and  
393 of all the rock magnetic parameters through the whole core, indicates that a geomagnetic origin  
394 of the ChRM oscillation recorded before the M-B transition is by far most likely and we  
395 conclude that the CADO core preserves a detailed record of the geomagnetic M-B precursor.

396

## 397 **5. Discussion and conclusion**

398 The collection of well defined paleomagnetic data at high-resolution throughout the study  
399 sequence, and the consequent compilation of detailed ChRM directions and RPI record, brought  
400 important contributions to the reconstruction of the geomagnetic field variability from high  
401 latitudes of the southern hemisphere, and therefore to the understanding of the key general  
402 features of the Earth's magnetic field within the polar regions.

403 The CADO RPI curve shows that paleointensity oscillations with periods longer than a few ka  
404 can be matched to the global RPI stacks and that a few sharp oscillations to anomalously low  
405 ChRM values, occurring during intervals of RPI lows, may represent the smoothed record of  
406 geomagnetic excursions or, alternatively, document the occurrence of only limited deviations  
407 from average paleomagnetic direction at the site location during the whole Brunhes Chron. In  
408 any case, on the whole the paleomagnetic record of the Brunhes Chron does not indicate a  
409 substantially larger variability of the geomagnetic field with respect to coeval records from  
410 intermediate and low latitudes with comparable sedimentation rates. This is in contrast with the  
411 larger variability reported for coeval sediment cores from the Arctic region [e.g. Nowaczyk and  
412 Antonow, 1997; Nowaczyk and Frederichs, 1999].

413 Though the relatively low geomagnetic variability and the relatively modest record of known  
414 geomagnetic excursions, the paleomagnetic record of the CADO core preserves a relatively  
415 detailed registration of the Matuyama-Brunhes reversal and supports the global existence of a  
416 precursor preceding by a few ka the full major reversal. As a result, this record represents the  
417 southernmost registration of the M-B transition and its precursor and indicates that the timing,  
418 rate and dynamics of such reversal and event, at high southern latitudes, are not substantially  
419 different from those reconstructed elsewhere.

420 In addition, orbital periodicities (100 ka and 41 ka) are found for the ChRM paleomagnetic  
421 inclination record, which are similar to those reported for other sedimentary cores at low-  
422 latitudes [Yamazaki and Oda 2002; 2004]. These data support the model of Yamazaki and Oda  
423 [2002], which suggests a connection between the geodynamo and the orbital eccentricity,  
424 indicating that long-term geomagnetic secular variation in inclination are controlled by changes  
425 in the relative strength of the geocentric axial dipole and persistent non-dipole components. The  
426 significant coherence between ChRM inclination variations and paleointensity ( $\text{NRM}_{20\text{mT}}/\kappa$ )  
427 are also similar to those obtained on a sediment core from the western equatorial Pacific by  
428 Yamazaki and Oda [2002; 2004] and indicates that shallower (steeper) inclinations may  
429 correlate with paleointensity minima (maxima).

430 Finally, rock magnetic data from the CADO core indicate a substantial uniformity of  
431 concentration, composition and grain size of the magnetic minerals contained in the study  
432 sequence. On the one hand, this uniformity is consistent with the observed homogeneity of  
433 sedimentary facies and indicates that the alternation of paleoclimatic phases that characterized  
434 the last ca 800 ka did not produce pronounced oscillations in the environmental magnetic  
435 proxies at the core location. This result matches the previous findings of Macri et al. [2005] for  
436 shorter cores from the WLB and indicates a substantial stability of the East Antarctic Ice Sheet  
437 during the middle and late Pleistocene. On the other hand, a climatic periodicity of 100 ka is  
438 detectable in the  $\kappa$  and  $\text{ARM}_{20\text{mT}}$  parameters, together with a minor contribution of the 41 ka

439 obliquity periodicity for the  $\kappa$  and  $\kappa\text{ARM}_{0\text{mT}}/\kappa$  parameters, indicating that subtle variations  
440 linked to orbital cycle affect the concentration and grain-size of the magnetic particles in the  
441 study sequence.

442

### 443 **Acknowledgments**

444 The MD03-2595 CADO core was studied as part of the QUASAR (QUaternary Sedimentary  
445 processes on the east Antarctic continental Rise) project that was funded by the PNRA  
446 (*Programma Nazionale di Ricerche in Antartide*). Members of the QUASAR working group are  
447 acknowledge for help with continued discussion on core stratigraphy and sedimentology. We  
448 thank two anonymous reviewers for their comments and suggestions, which allowed to improve  
449 the manuscript.

450

### 451 **References**

452 Arason, P., and Levi, S., 1990. Compaction and inclination shallowing in deep-sea sediments  
453 from the Pacific Ocean. *J. Geophys. Res.*, 95: 4501–4510.

454

455 Aurnou, J.M., Andreadis, S., Zhu, L., and Olson, P.L., 2003. Experiments on convection in  
456 Earth's core tangent cylinder. *Earth Planet. Sci. Lett.*, 212: 119-134.

457

458 Biggin, A.J., Strik, G.H.M.A., and Langereis C.G., 2009. The intensity of the geomagnetic field  
459 in the late-Archaeon: new measurements and an analysis of the updated IAGA palaeointensity  
460 database. *Earth Planets Space*, 61: 9–22.

461

462 Brachfeld, S.A., Acton, G.D., Guyodo, Y., and Banerjee, S.K., 2000. High-resolution  
463 paleomagnetic records from Holocene sediments from the Palmer Deep, western Antarctic  
464 Peninsula. *Earth Planet. Sci. Lett.*, 181: 421-441.

465

466 Brachfeld, S.A., Domack, E.W., Kissel, C., Laj, C., Leventer, A., Ishman, S.E., Gilbert, R.,  
467 Camerlenghi, A., and Eglinton, L.B., 2003. Holocene History of the Larsen Ice Shelf  
468 Constrained by Geomagnetic Paleointensity Dating, *Geology*, 31: 749-752.

469

470 Brancolini, G., and Harris, P.T., 2000. Post Cruise Report AGSO Survey 217: Joint  
471 Italian/Australian Marine Geoscienze Expedition Aboard the R.V. Tangaroa to the Geotge Vth  
472 Land Region of East Antartica during February-March, 2000. Australian National Antarctic  
473 Research Expeditions Project No. 1044, Wilkes Land Glacial History (WEGA), AGSO Record.

474

475 Brown, L.L., Singer, B.S., Pickens, J.C., and Jicha, B.R. 2004. Paleomagnetic directions and  
476  $^{40}\text{Ar}/^{39}\text{Ar}$  ages from the Tatara-San Pedro volcanic complex, Chilean Andes: Lava record of a  
477 Matuyama-Brunhes precursor? *Journal of Geophys. Res.*, Vol. 109, B12101,  
478 doi:10.1029/2004JB003007.

479

480 Busetti, M., Caburlotto, A., Armand, L., Damiani, D., Giorgetti, G., Lucchi, R.G., Quilty, P.G.,  
481 and Villa, G., 2003. Plio-Quaternary sedimentation on the Wilkes land continental rise:  
482 preliminary results. *Deep-Sea Research II*, 50: 1529–1562.

483

484 Caburlotto, A., Macrì, P., Damiani, D., Giorgetti, G., Busetti, M., Villa, G., and Lucchi, R.G.,  
485 2003. Piston cores from the Wilkes Land Rise: Data and Considerations. *Terra Antartica*  
486 *Reports*, 9: 63-68.

487

488 Channell, J.E.T., Curtis, J.H., and Flower, B.P., 2004. The Matuyama-Brunhes boundary  
489 interval (500-900 ka) in North Atlantic drift sediments. *Geophys. J. Int.*, 158: 489-505.

490

491 Channell, J.E.T., 2006. Late Brunhes polarity excursions (Mono Lake, Iceland Basin and  
492 Pringle Falls) recorded at ODP Site 919 (Irminger Basin). *Earth Planet. Sci. Lett.*, 244: 378-393.

493

494 Channell, J.E.T., Xuan C., and Hodell, D.A., 2009. Stacking paleointensity and oxygen isotope  
495 data for the last 1.5 Myr (PISO-1500). *Earth Planet. Sci. Lett.*, 283: 14-23.

496

497 Clement, B.M., 2004. Dependence of the duration of geomagnetic polarity reversals on site  
498 latitude. *Nature*, 428: 637-640.

499

500 Coe, R.S., Singer, B.S., Pringle, M.S., and Zhao X., 2004. Matuyama–Brunhes reversal and  
501 Kamikatsura event on Maui: paleomagnetic directions,  $^{40}\text{Ar}/^{39}\text{Ar}$  ages and implications. *Earth*  
502 *Plan. Sci. Lett.*, 222: 667-684.

503

504 Day, R., Fuller, M., and Schmidt, V.A., 1977. Hysteresis properties of titanomagnetites. Grain-  
505 size and compositional dependence. *Phys. Earth Planet. Int.*, 13: 260–267.

506

507 Deamer, G.A., and Kodama, K.P., 1990. Compaction-induced inclination shallowing in  
508 synthetic and natural clay-rich sediments. *J. Geophys. Res.*, 95(B4): 4511-4529.

509

510 deMenocal, P.B., Ruddiman W.F., and Kent D.V., 1990. Depth of post-depositional remanence  
511 acquisition in deep-sea sediments: a case study of the Brunhes-Matuyama reversal and oxygen  
512 isotopic Stage 19.1. *Earth and Planet. Sci. Lett.*, 99: 1-13.

513

514 Dinarès-Turell, J., Sagnotti, L., and Roberts, A.P., 2002. Relative geomagnetic paleointensity  
515 from the Jaramillo Subchron to the Matuyama/Brunhes boundary as recorded in a  
516 Mediterranean piston core. *Earth Planet. Sci. Lett.*, 194: 327-341.

517

518 Escutia, C., Eittreim, S.L., and Cooper, A.K., 1997. Cenozoic Sedimentation on the Wilkes  
519 Land Continental Rise, Antarctica. In C.A., Ricci (Ed.) *Proceedings of the VII International  
520 Symposium on Antarctic Earth Sciences*. Terra Antarctica Publication, Siena: 791-795.

521

522 Fisher, R.A., 1953. Dispersion on a sphere. *Proc. R. Soc. London*, 217: 295-305.

523

524 Glatzmaier, G.A., and Roberts, P.H., 1995a. A three-dimensional convective dynamo solution  
525 with rotating and finitely conducting inner core and mantle. *Phys. Earth Planet. Int.*, 91: 63-75.

526

527 Glatzmaier, G.A., and Roberts, P.H., 1995b. A Three-Dimensional Self-Consistent Computer  
528 Simulation of a Geomagnetic Field Reversal. *Nature*, 377: 203-209.

529

530 Guillou, H., Singer, B., Laj, C., Kissel, C., Scaillet, S., and Jicha, B.R., 2004. On the age of the  
531 Laschamp geomagnetic excursion. *Earth Planet. Sci. Lett.*, 227: 331–343.

532

533 Guyodo, Y., and Valet, J.-P., 1999. Global changes in geomagnetic intensity during the past 800  
534 thousand years. *Nature*, 399: 249-252.

535

- 536 Guyodo, Y., Acton, G.D., Brachfeld, S., and Channell, J.E.T., 2001. A sedimentary  
537 paleomagnetic record of the Matuyama chron from the Western Antarctic Margin (ODP Site  
538 1101). *Earth Planet. Sci. Lett.* 191:61–74.
- 539
- 540 Guyodo, Y., Channell, J.E.T. and Thomas Ray, G., 2002. Deconvolution of u-channel  
541 paleomagnetic data near geomagnetic reversals and short events. *Geoph. Res. Lett.*, 29, 1845,  
542 doi: 10.1029/2002GL014927.
- 543
- 544 Hartl, P., and Tauxe, L., 1996. A precursor to the Matuyama/Brunhes transition-field instability  
545 as recorded in pelagic sediments. *Earth Plan. Sci. Lett.*, 138: 121-135.
- 546
- 547 Hyodo, M., Biswas, D.K., Noda, T., Tomioka, N., Mishima, T., Itota, C., and Sato, H., 2006.  
548 Millennial- to submillennial-scale features of the Matuyama-Brunhes geomagnetic polarity  
549 transition from Osaka Bay, southwestern Japan. *J. Geophys. Res.*, 111, B02103,  
550 doi:10.1029/2004JB003584.
- 551
- 552 Kent, D.V., and Schneider, D.A., 1995. Correlation of paleointensity variation records in the  
553 Brunhes/Matuyama polarity transition interval. *Earth Planet. Sci. Lett.*, 129: 135-144.
- 554
- 555 King, J.W., Banerjee, S.K., and Marvin, J., 1983. A new rock-magnetic approach to selecting  
556 sediments for geomagnetic paleointensity for the last 4000 years. *J. Geophys. Res.*, 88(B7):  
557 5911-5921.
- 558
- 559 Kirschvink, J.L., 1980. The least-squares line and plane and the analysis of paleomagnetic data.  
560 *Geophys. J. Roy. Astron. Soc.*, 62: 699-718.
- 561
- 562 Kuang, W., and Bloxham, J., 1997. An Earth-like numerical dynamo model. *Nature*, 389: 371-  
563 374.
- 564
- 565 Langereis, C.G., Dekkers, M.J., de Lange, G.J., Paterne, M.E., and van Santvoort, P.J.M., 1997.  
566 Magnetostratigraphy and astronomical calibration of the last 1.1 Myr from an eastern  
567 Mediterranean piston core and dating of short events in the Brunhes. *Geophys. J. Int.*, 129: 75-  
568 94.
- 569

- 570 Lawrence, K. P., Tauxe, L., Staudigel, H., Constable, C.G., Koppers, A., McIntosh, W., and  
571 Johnson C.L., 2009. Paleomagnetic field properties at high southern latitude, *Geochem.*  
572 *Geophys. Geosyst.*, 10, Q01005, doi:10.1029/2008GC002072.
- 573
- 574 Lund, S.P., and Keigwin, L., 1994. Measurement of the degree of smoothing in sediment  
575 paleomagnetic secular variation records: an example from Late Quaternary deep-sea sediments  
576 of the Bermuda Rise, western North Atlantic Ocean. *Earth Planet. Sci. Lett.*, 122: 317–330.
- 577
- 578 Lund, S.P., Acton, G., Clement, B., Hastedt, M., Okada, M., and Williams, R., 1998.  
579 Geomagnetic field excursions occurred often during the last million years. *EOS, Trans. Am.*  
580 *Geophys. Un.*, 79: 178-179.
- 581
- 582 Macrì, P., Sagnotti, L., Dinares-Turell, J., and Caburlotto, A., 2005. A composite record of Late  
583 Pleistocene relative geomagnetic paleointensity from the Wilkes Land Basin (Antarctica). *Phys.*  
584 *Earth Planet. Int.*, 151: 223–242.
- 585
- 586 Macrì, P., Sagnotti, L., and Lucchi, R.G., 2006. A stacked record of relative geomagnetic  
587 paleointensity for the past 270 kyr from the western continental rise of the Antarctic Peninsula.  
588 *Earth Planet. Sci. Lett.*, 252: 162-179.
- 589
- 590 Meynadier, L., Valet, J.-P., Weeks, R., Shackleton, N.J., and Hagee, V.L., 1992. Relative  
591 geomagnetic intensity of the field during the last 140 ka. *Earth Planet. Sci. Lett.*, 114: 39-57.
- 592
- 593 Mitra, R. and Tauxe, L., 2009. Full vector model for magnetization in sediments. *Earth Planet.*  
594 *Sci. Lett.*, 286: 535-545.
- 595
- 596 Nowaczyk, N.R., and Antonow, M., 1997. High resolution magnetostratigraphy of four  
597 sediment cores from the Greenland Sea - I. Identification of the Mono Lake excursion,  
598 Laschamp and Biwa I/Jamaica geomagnetic polarity events. *Geophys. J. Int.*, 131: 310–324.
- 599
- 600 Nowaczyk, N., and Frederichs, T., 1999. Geomagnetic events and relative paleointensity  
601 variations during the last 300 ka as recorded in Kolbeinsey Ridge sediments, Iceland Sea,  
602 indication for a strongly variable geomagnetic field. *Int. J. Earth Sci.*, 88: 116–131.
- 603



- 604 Oda, H., and Shibuya, H., 1996. Deconvolution of long-core paleomagnetic data of Ocean  
605 Drilling Program by Akaike's Bayesian Information Criterion minimization. *J. Geophys. Res.*,  
606 101: 2815-2834.
- 607
- 608 Paillard, D., Labeyrie, L., and Yiou, P., 1996. Macintosh program performs time-series analysis.  
609 *Eos, Trans. Am. Geophys. Un.*, 77: 397.
- 610
- 611 Perrin, M., and Schnepf, E., 2004. IAGA paleointensity database: Distribution and quality of  
612 the data set. *Phys. Earth Planet. Int.*, 147(2-3): 255-267.
- 613
- 614 Quidelleur, X., Carlut, J., Soler, V., Valet, J.-P., and Gillot, P.-Y., 2003. The age and duration  
615 of the Matuyama-Brunhes transition from new K-Ar data from La Palma (Canary Islands) and  
616 revisited  $^{40}\text{Ar}/^{39}\text{Ar}$  ages. *Earth Planet. Sci. Lett.*, 208: 149-163.
- 617
- 618 Rebesco, M., Larter, R.D., Barker, P.F., Camerlenghi, A., and Vanneste, L.E., 1997. The history  
619 of sedimentation on the continental rise west of the Antarctic Peninsula. In Cooper A.K. and  
620 P.F. Barker (Eds), *Geology and seismic stratigraphy of the Antarctic margin, Part 2. Antarctic*  
621 *Research Series 71*, American Geophysical Union, Washington DC: 29-49.
- 622
- 623 Roberts, A.P., and Winklhofer, M., 2004. Why are geomagnetic excursions not always recorded  
624 in sediments? Constraints from post-depositional remanent magnetization lock-in modelling.  
625 *Earth Planet. Sci. Lett.*, 227: 345-359.
- 626
- 627 Roberts, A.P., 2006. High-resolution magnetic analysis of sediment cores: Strengths, limitations  
628 and strategies for maximizing the value of long-core magnetic data, *Phys. Earth Planet. Int.*,  
629 156: 162-178.
- 630
- 631 Roberts, A.P., 2008. Geomagnetic excursions: knowns and unknowns. *Geophys. Res. Lett.*, 35,  
632 L17307, doi:10.1029/2008GL034719.
- 633
- 634 Sagnotti, L., Macrì, P., Camerlenghi, A., and Rebesco M., 2001. Environmental magnetism of  
635 late Pleistocene sediments from the Pacific margin of the Antarctic Peninsula and  
636 interhemispheric correlation of climatic events. *Earth Planet. Sci. Lett.*, 192: 65-80.
- 637

- 638 Sagnotti, L., Rochette, P., Jackson, M., Vadeboin, F., Dinarès-Turell, J., Winkler, A., and  
639 “Mag-Net” Science Team, 2003. Inter-laboratory calibration of low field magnetic and  
640 anhysteretic susceptibility measurements. *Phys. Earth Planet. Int.*, 138: 25–38.  
641
- 642 Sagnotti, L., Budillon, F., Dinarès-Turell, J., Iorio, M., and Macrì, P., 2005. Evidence for a  
643 variable paleomagnetic lock-in depth in the Holocene sequence from the Salerno Gulf (Italy):  
644 implications for “high-resolution” paleomagnetic dating, *Geochem. Geophys. Geosyst.*, 6,  
645 doi:10.1029/2005GC001043.  
646
- 647 Singer, B.S., Relle, M.K., Hoffman, K.A., Battle, A., Laj, C., Guillou, H., and Carracedo J.C.,  
648 2002. Ar/Ar ages from transitionally magnetized lavas on La Palma, Canary Islands, and the  
649 geomagnetic instability timescale. *J. Geophys. Res.*, 107: 2307, doi: 10.1029/2001JB001613.  
650
- 651 Singer, B.S., Jicha, B.R., Kirby, B.T., Geissman, J.W., and Herrero-Bervera, E., 2008.  
652 40Ar/39Ar dating links Albuquerque Volcanoes to the Pringle Falls excursion and the  
653 Geomagnetic Instability Time Scale. *Earth Planet. Sci. Lett.*, 267: 584–595.  
654
- 655 Spassov, S., Heller, F., Evans, M.E., Yue, L.P., von Dobeneck, T., 2003. A lock-in model for  
656 the complex Matuyama-Brunhes boundary record of the loess/palaeosol sequence at Lingtai  
657 (Central Chinese Loess Plateau). *Geophys. J. Int.*, 155, (2): 350-366.  
658
- 659 Stacey, F.D., and Banerjee, S.K., 1974. *The physical principles of rock magnetism*. Elsevier,  
660 Amsterdam, 195 p.  
661
- 662 Stoner, J.S., Laj, C., Channell, J.E.T., and Kissel, C., 2002. South Atlantic and North Atlantic  
663 geomagnetic paleointensity stacks (0-80 ka): implications for inter-hemispheric correlation.  
664 *Quat. Sci. Rev.*, 21:1141-1151.  
665
- 666 Stoner, J.S., Channell, J.E.T., Hodell, D.A., and Charles, C.D., 2003. A ~570-kyr geomagnetic  
667 paleosecular variation record from the sub-Antarctic South Atlantic (ODP Site 1089). *J.*  
668 *Geophys. Res.*, 108 (B5):2242, doi:10.1029/2001JB001390  
669
- 670 Sugiura, N., 1979. ARM, TRM and magnetic interactions: concentration dependence, *Earth*  
671 *Planet. Sci. Lett.*, 42: 451-455.

672

673 Tan, X.D., Kodama, K.P., Chen, H.L., Fang, D.J., Sun, D.J., and Li, Y.A., 2003.  
674 Paleomagnetism and magnetic anisotropy of Cretaceous red beds from the Tarim basin,  
675 northwest China: Evidence for a rock magnetic cause of anomalously shallow paleomagnetic  
676 inclinations from central Asia. *J. Geophys. Res.*, 108, 2107, doi:10.1029/2001JB001608.

677

678 Tarduno, J.A., and Wilkison, S.L., 1996. Non-steady state magnetic mineral reduction, chemical  
679 lock-in, and delayed remanence acquisition in pelagic sediments. *Earth Planet. Sci. Lett.*, 144:  
680 315-326.

681

682 Tauxe, L., and Kent, D.V., 1984. Properties of a detrital remanence carried by haematite from  
683 study of modern river deposits and laboratory redeposition experiments. *Geophys. J. R. Astr.*  
684 *Soc.*, 77: 543–561.

685

686 Tauxe, L., 1993. Sedimentary records of relative paleointensity of the geomagnetic field: theory  
687 and practice. *Rev. Geophys.*, 31: 319-354.

688

689 Tauxe, L., Herbert, T., Shackleton, N.J., and Kok, Y.S., 1996. Astronomical calibration of the  
690 Matuyama-Brunhes boundary: Consequences for magnetic remanence acquisition in marine  
691 carbonates and the Asian loess sequences. *Earth Planet. Sci. Lett.*, 140: 133–146.

692

693 Tauxe, L., and Kent, D.V., 2004. A simplified statistical model for the geomagnetic field and  
694 the detection of shallow bias in paleomagnetic inclinations: Was the ancient magnetic field  
695 dipolar? In *Timescales of the Paleomagnetic field*, Channell, J.E.T. et al., eds., *Geophysical*  
696 *Monograph*, 145: 101-116.

697

698 Thouveny, N., Carcaillet, J., Moreno, E., Leduc, G., and Nérini, D., 2004. Geomagnetic moment  
699 variation and paleomagnetic excursions since 400 ka BP: a stacked record of sedimentary  
700 sequences of the Portuguese margin. *Earth Planet.Sci.Lett.*, 219: 377-396.

701

702 Tauxe L (2006) Long term trends in paleointensity: The contribution of DSDP/ODP submarine  
703 basaltic glass collections. *Physics of the Earth and Planetary Interiors*, 156: 223–241.

704

- 705 Tauxe, L., and Yamazaki, T., 2007. Paleointensities. In Schubert, G., (Ed.), Treatise on  
706 Geophysics, vol.5, Geomagnetism. Elsevier Ltd, Oxford: 509–564.  
707
- 708 Thouveny, N., Bourlès, D.L., Saracco, G., Carcaillet, J.T., and Bassinot, F., 2008. Paleoclimatic  
709 context of geomagnetic dipole lows and excursions in the Brunhes, clue for an orbital influence  
710 on the geodynamo? *Earth Planet. Sci. Lett.*, 275: 269-284.  
711
- 712 Tric, E., Laj, C., Valet, J.-P., Tucholka, P., Paterne, M., and Gichard, F., 1991. The Blake  
713 geomagnetic event: transition geometry, dynamical characteristics and geomagnetic  
714 significance. *Earth Planet. Sci. Lett.*, 102: 1-13.  
715
- 716 Valet, J.P., Meynadier, L., Bassinot, F.C., and Garnier, F., 1994. Relative paleointensity across  
717 the last geomagnetic reversal from sediments of the Atlantic, Indian and Pacific Oceans. *Geoph.*  
718 *Res. Lett.*, 21(6): 485-488.  
719
- 720 Valet, J.-P., and Meynadier, L., 1998. A comparison of different techniques for relative  
721 paleointensity. *Geophys. Res. Lett.*, 25: 89-92.  
722
- 723 van Vreumingen, M.J., 1993a. The Influence of Salinity and Flocculation Upon the Acquisition  
724 of Remanent Magnetization in Some Artificial Sediments. *Geophys. J. Int.* 114 (3), 607–614.  
725
- 726 van Vreumingen, M.J., 1993b. The Magnetization Intensity of Some Artificial Suspensions  
727 While Flocculating in a Magnetic-Field. *Geophys. J. Int.* 114 (3), 601–606.  
728
- 729 Zhu, R.X., Zhou, L.P., Laj, C., Mazaud, A., and Ding, Z.L., 1994. The Blake geomagnetic  
730 episode recorded in Chinese loess. *Geophys. Res. Lett.*, 21: 697-700.  
731
- 732 Yamazaki, T., and Ioka, N., 1997. Cautionary note on magnetic grain-size estimation using the  
733 ratio of ARM to magnetic susceptibility. *Geophys. Res. Lett.*, 24: 751-754.  
734
- 735 Yamazaki, T., and Oda, H., 2001. A Brunhes-Matuyama polarity transition record from anoxic  
736 sediments in the South Atlantic (Ocean Drilling Program Hole 1082C). *Earth Planets Space*, 53:  
737 817-827.  
738

739 Yamazaki, T., and Oda, H., 2002. Orbital influence on Earth's magnetic field: 100,000-year  
740 periodicity in inclination. *Science*, 295: 2435-2438.

741

742 Yamazaki, T., and Oda H., 2004. Intensity-Inclination Correlation on Long-Term Secular  
743 Variation of the Geomagnetic Field and its Relevance to Persistent Non-Dipole Component.  
744 AGU Monograph 145 "Timescales of the Internal Geomagnetic Field": 287-298.

745

746 Yamazaki, T., 2008. Magnetostatic interactions in deep-sea sediments inferred from first-order  
747 reversal curve diagrams: Implications for relative paleointensity normalization. *Geochem.*  
748 *Geophys. Geosyst.*, 9, doi: Q02005, doi:10.1029/2007GC001797.

749

750

### 751 **Figure captions**

752 Fig. 1 – A) Bathymetric map of the continental rise of the Wilkes Land Basin: the morphology  
753 of the rise is characterized by a channel-ridge system elongated perpendicular to the margin.  
754 Points aligned on acoustic Line 26 shows the location of the previously studied WEGA cores  
755 (see text). B) 3.5 kHz acoustic profile crossing the Buffon Canyon (Line W39) with location of  
756 the MD03- 2595 core. Redrawn from Buseti et al. (2003).

757

758 Fig. 2 – Typical alternating field (AF) demagnetization behavior at selected depths of the  
759 MD03- 2593 core. Paleomagnetic data indicate that, after removal of a viscous component at  
760  $AF < 10\text{-}20$  mT, a characteristic remanent magnetization (ChRM) can be easily identified.  
761 Orthogonal vector diagrams: open and closed symbols represent projections onto vertical and  
762 horizontal planes, respectively. Equal area projections: open (close) symbols represent  
763 projection onto the upper (lower) hemisphere.

764

765 Fig. 3 – Paleomagnetic directions, maximum angular deviation (MAD) [Kirschvink, 1980] and  
766 the normalized relative paleointensity curves  $NRM_{20mT}/\kappa$  and  $NRM_{20mT}/ARM_{20mT}$  for the  
767 CADO core. The u-channel sections (1 to 24) are indicated to the right of the lithostratigraphic  
768 column. The dashed lines on the ChRM declination and inclination plots indicate the expected  
769 value of the declination ( $360^\circ$ ) and inclination ( $-76.8^\circ$ ) at the core location.

770

771 Fig. 4 – Downcore variation of the main rock magnetic parameters measured for the CADO  
772 core. The little squares on the right of the lithostratigraphic column indicate the position of the 8

773 sub-samples selected for rock magnetic analysis. Horizontal gray bars in the plots indicate the  
774 position of silty clays and laminated muds.

775

776 Fig. 5 – Thermomagnetic curves of the samples selected for rock magnetic analyses, showing the  
777 variation in the magnetic susceptibility ( $\kappa$ ) with temperature in heating-cooling cycles from  
778 room temperature to 700°C. The sharp drop at ca 580°C in all the heating curves indicates the  
779 presence of magnetite, whereas the thermal instability between 250 and 350°C suggests the  
780 presence of maghemite which is converted to hematite during the thermal treatment. The  
781 cooling path is always well above of the heating path and indicates that new magnetite is  
782 produced by thermal alteration during heating.

783

784 Fig. 6 - A) and B) Representative hysteresis loops and C)  $B_{cr}/B_c$  vs  $M_r/M_s$  plot [Day et al. 1977]  
785 for the selected specimens of the CADO core.  $B_{cr}$ : remanent coercive force,  $B_c$ : coercive force,  
786  $M_r$ : saturation remanent magnetization,  $M_s$ : saturation magnetization. Hysteresis parameters  
787 were computed after correction for the high-field paramagnetic slope. SD= single domain,  
788 PSD= pseudo single domain, and MD= multidomain grains.. D) The ARM/ $\kappa$  ratio, indicates a  
789 substantial uniformity in magnetic mineral grain size, apart from a few data from distinct  
790 intervals, which were disregarded for RPI analyses

791

792 Fig. 7 – SINT-800 reference curve of Guyodo and Valet [1999] and the CADO RPI record  
793 ( $NRM_{20mT}/k$ ). Vertical lines indicate tie points used for correlation. B) After correlation the  
794 CADO RPI curve was scaled to its maximum value and plotted together with the SINT-800.  
795 The correlation indicates that the CADO core reaches back to ca 800 ka. C) Downcore variation  
796 of the sedimentation rates obtained with the RPI-based age model for the CADO core.  
797 Unbroken line is age versus depth, broken line is depth versus sedimentation rate calculated  
798 between the RPI tie points.

799

800 Fig. 8 – Comparison of the CADO RPI curve with the SINT-800 and the PISO-1500 global RPI  
801 stacks and with other southern high-latitude RPI records extracted from the MagIC database, in  
802 the interval 0-800 ka. Sint-800 from Guyodo and Valet, [1999], PISO-1500 from Channell et  
803 al., [2009], Core 1089 from Stoner et al. [2003], Ks87-752 from Valet et al. [1994], 5-pc01 from  
804 Stoner et al. [2002], Core 1101 from Guyodo et al. [2001], Core PC20 from Macrì et al. [2005].

805

806 Fig. 9 – Spectral analysis performed using Blackman-Tukey method with a Bartlett window. A)  
807 Square coherence and phase for the RPI curves with respect to each other and with respect to  
808 the normalization parameters. B) Square coherence and phase for the ChRM inclination with  
809 respect to the  $\text{NRM}_{20\text{mT}}/\kappa$  RPI record and the  $\text{ARM}_{0\text{mT}}/\kappa$  ratio, and for the  $\text{NRM}_{20\text{mT}}/\kappa$  RPI  
810 record with respect to the  $\text{ARM}_{0\text{mT}}/\kappa$  ratio and the reference SINT-800 stack. B) Square  
811 coherence and phase between CADO and PISO-1500 RPI records. See text for explanation.

812

813 Fig. 10 – Standard spectra of the parameters used for the RPI normalisation ( $\kappa$  and ARM), the  
814 normalized relative paleointensity curves ( $\text{NRM}_{20\text{mT}}/\kappa$  and  $\text{NRM}_{20\text{mT}}/\text{ARM}_{20\text{mT}}$ ),  $\text{ARM}_{0\text{mT}}/\kappa$  and  
815 the ChRM inclination.

816

817 Fig. 11 – A) Histograms of ChRM inclinations and declinations. N is the number of data.  
818 Expected normal and reverse inclinations at the CADO latitude site are shown as a vertical  
819 dashed lines. B) Equal-area projections of paleomagnetic directions. D and I are mean  
820 declination and inclination calculated using Fisher's statistics [Fisher 1953] on the not-  
821 transitional and not-excursion normal and reverse ChRM directions (i.e. directions providing a  
822 VGP latitude greater than  $\pm 45^\circ$ ), with uncertainties estimated by the  $\alpha_{95}$  parameter.

823

824 Fig. 12 – CADO RPI record and SINT-800 of Guyodo and Valet [1999], compared with ChRM  
825 inclination record and VGP latitude of the CADO core. The black arrows indicate geomagnetic  
826 excursions recognized in the literature, with the validated excursions, *sensu* Roberts [2008],  
827 indicated in bold (see text). The grey vertical areas correspond to the main RPI minima in the  
828 SINT-800 record of Guyodo and Valet [1999].

829

830 Fig. 13 – ChRM directions, MAD and VGP latitude for the bottom part of the CADO core  
831 (interval dated at 750-800 ka). Vertical dashed lines correspond to the u-channel breaks. The  
832 gray area shows the interval that was correlated to the uppermost part of the reverse Matuyama  
833 Chron preserving a record of the Matuyama-Brunhes transition and of its precursor. See text for  
834 discussion.

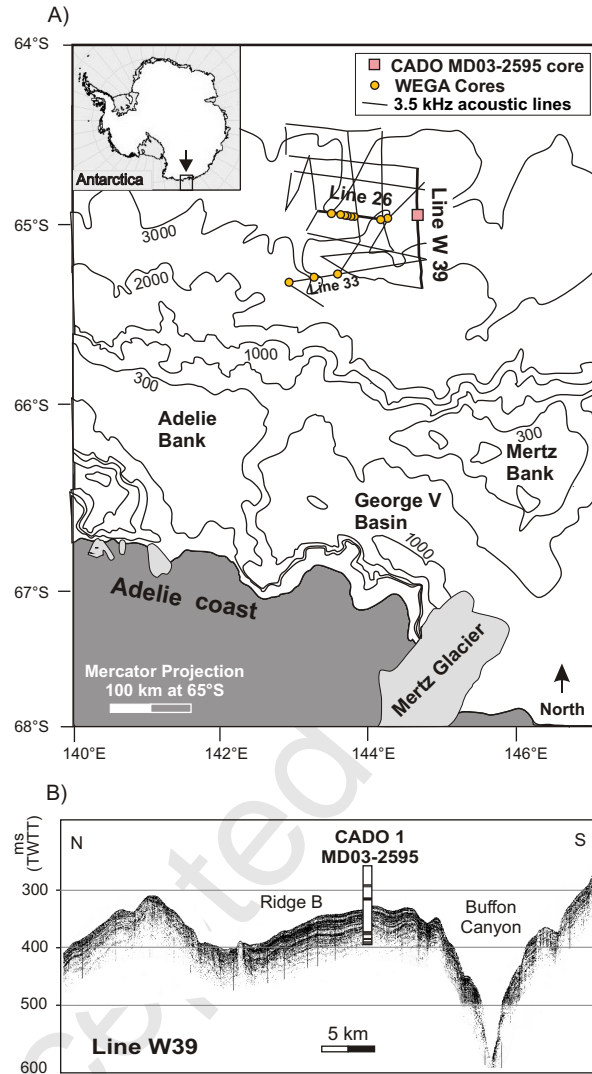


Fig. 1



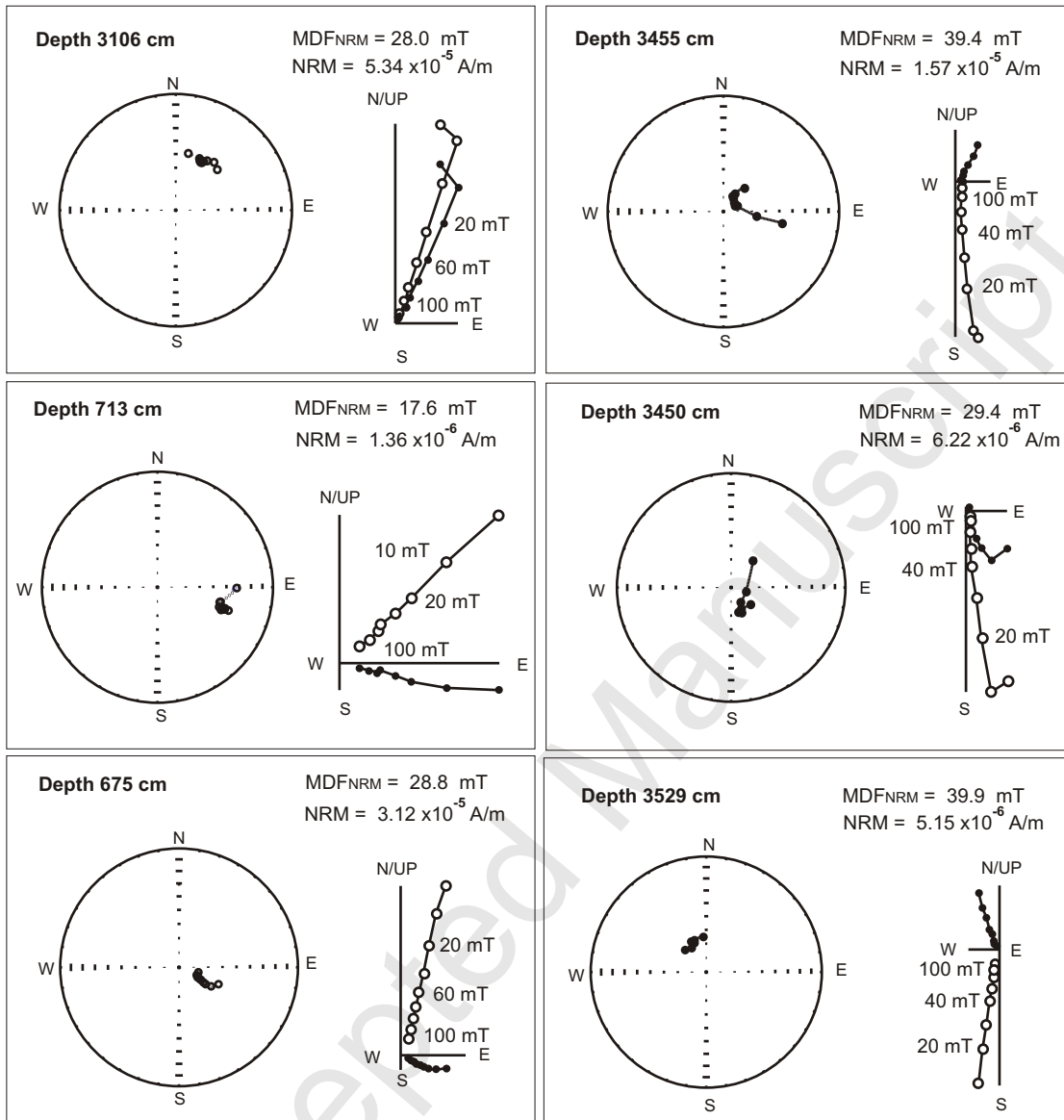


Fig. 2

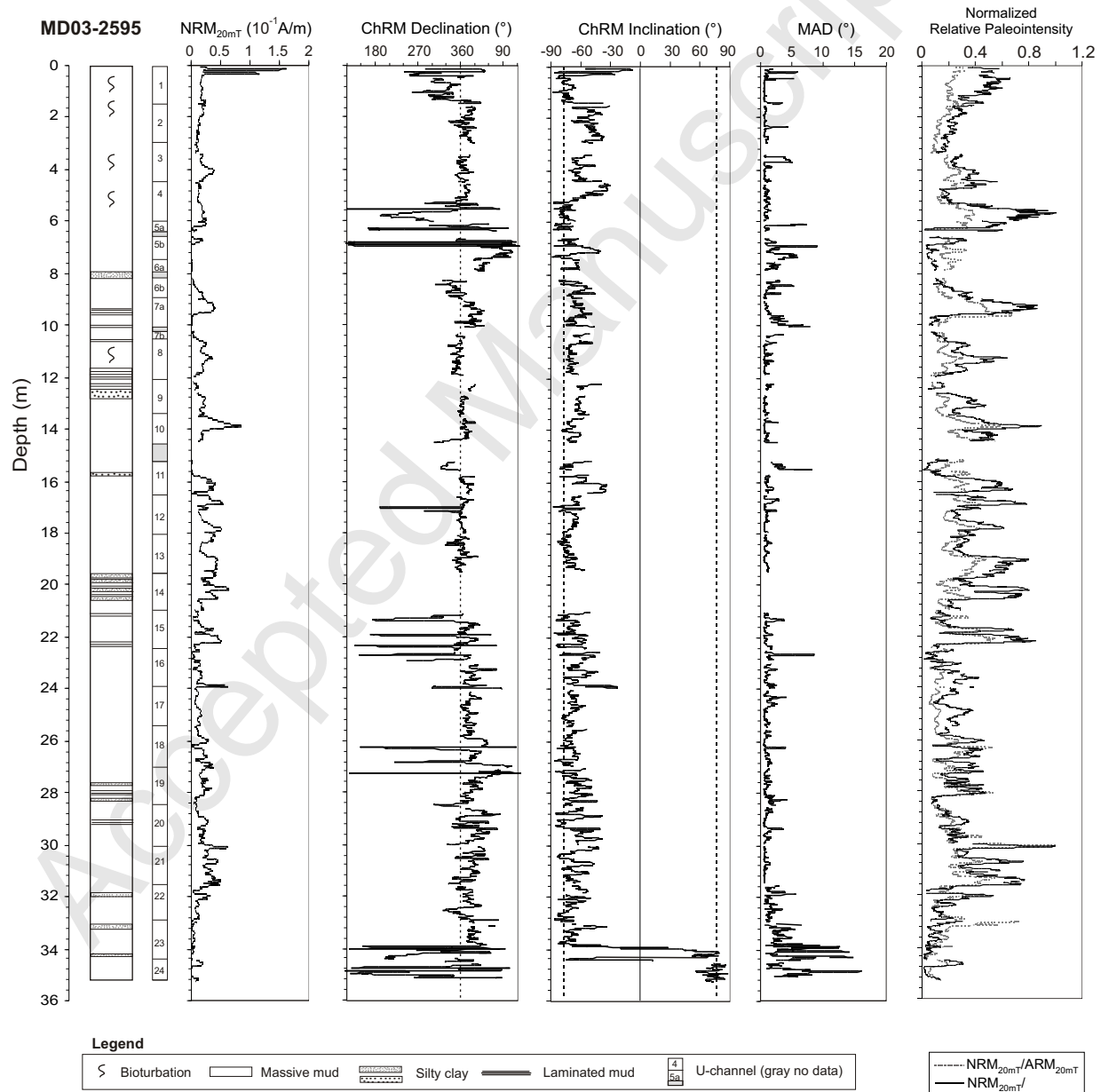


Fig. 3

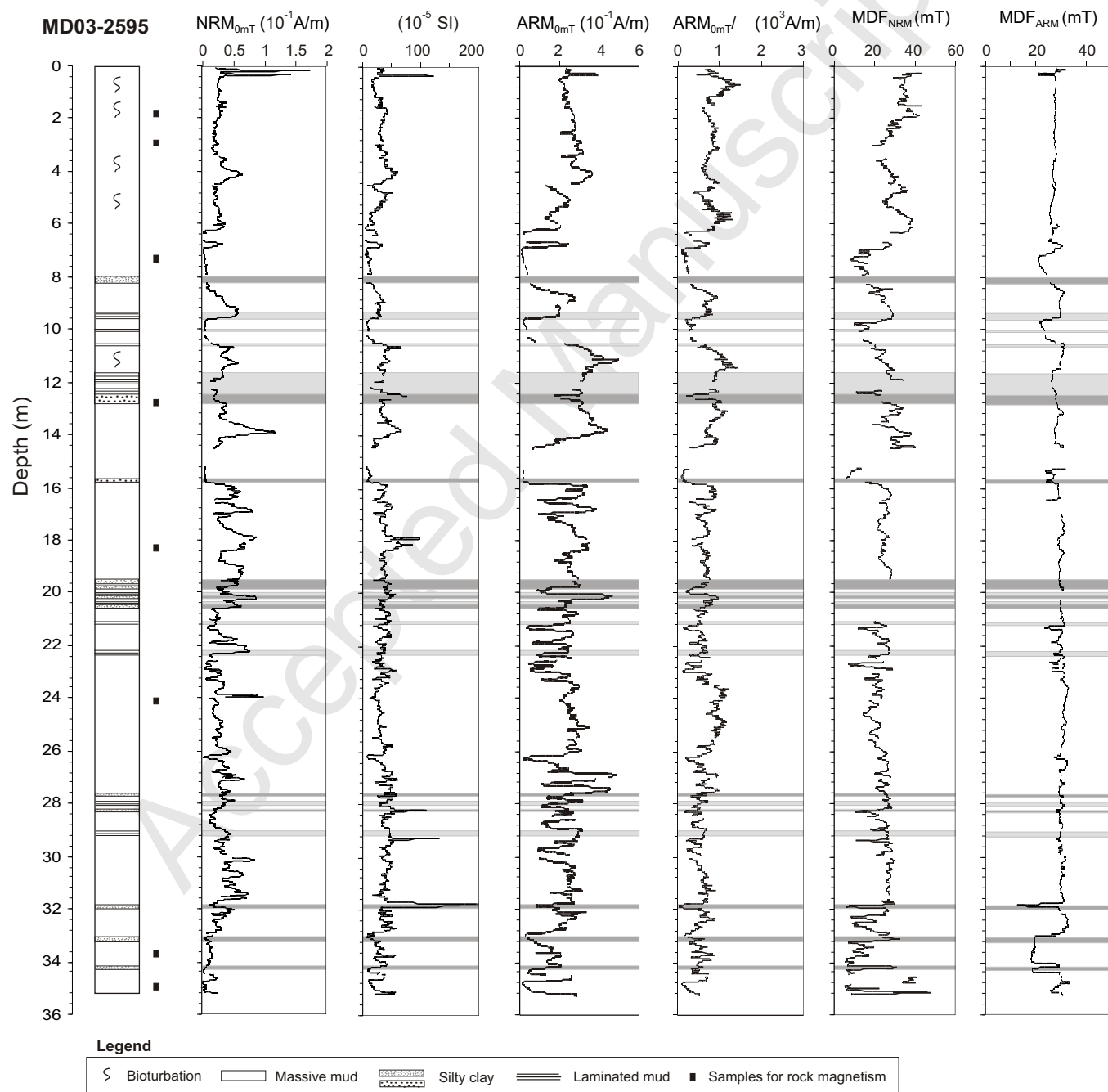


Fig. 4

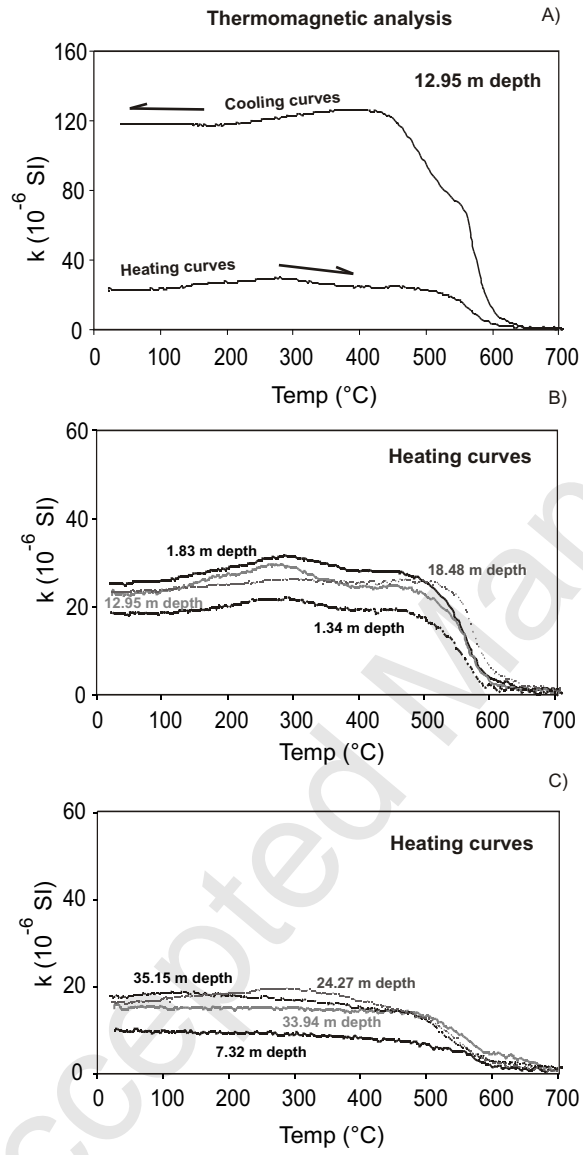


Fig. 5

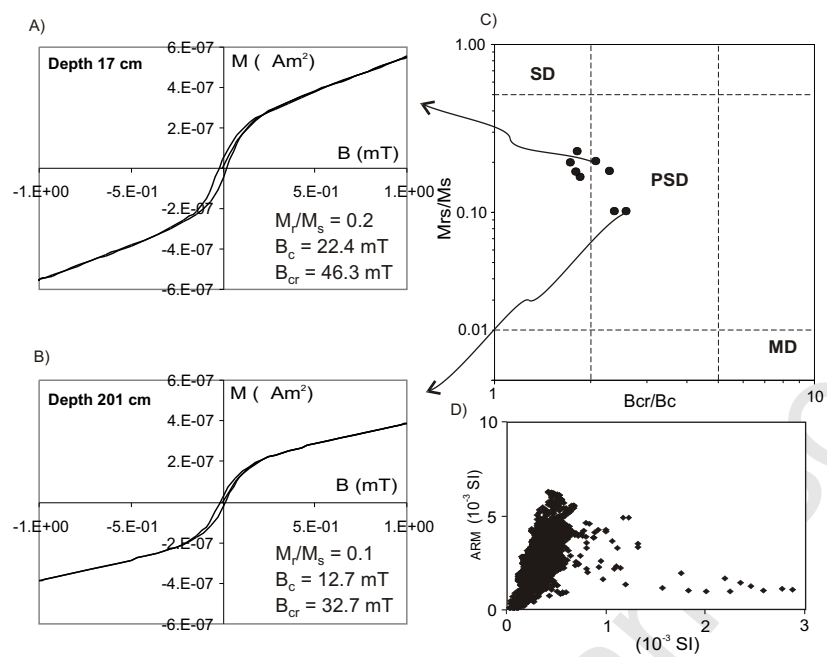


Fig. 6

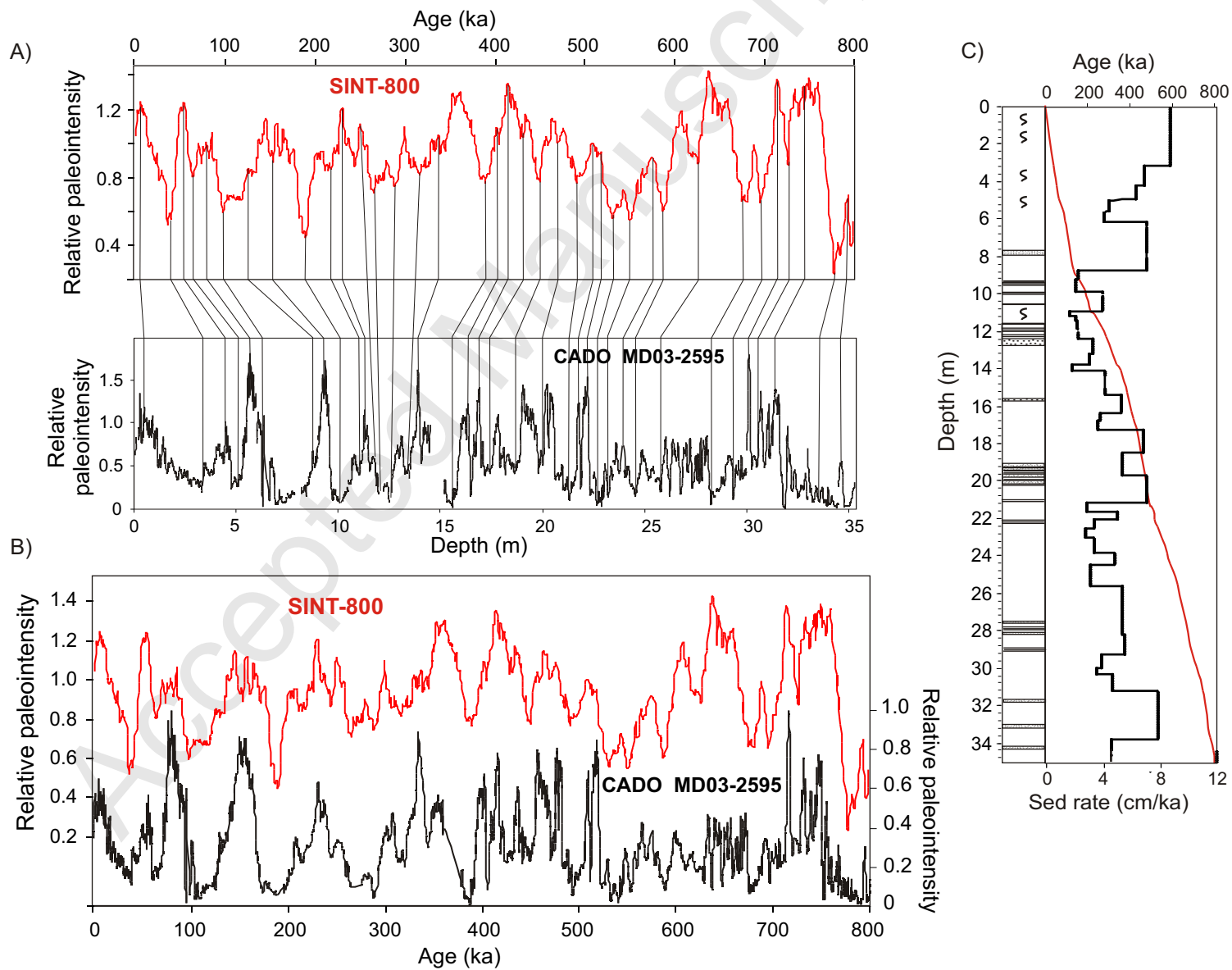


Fig. 7

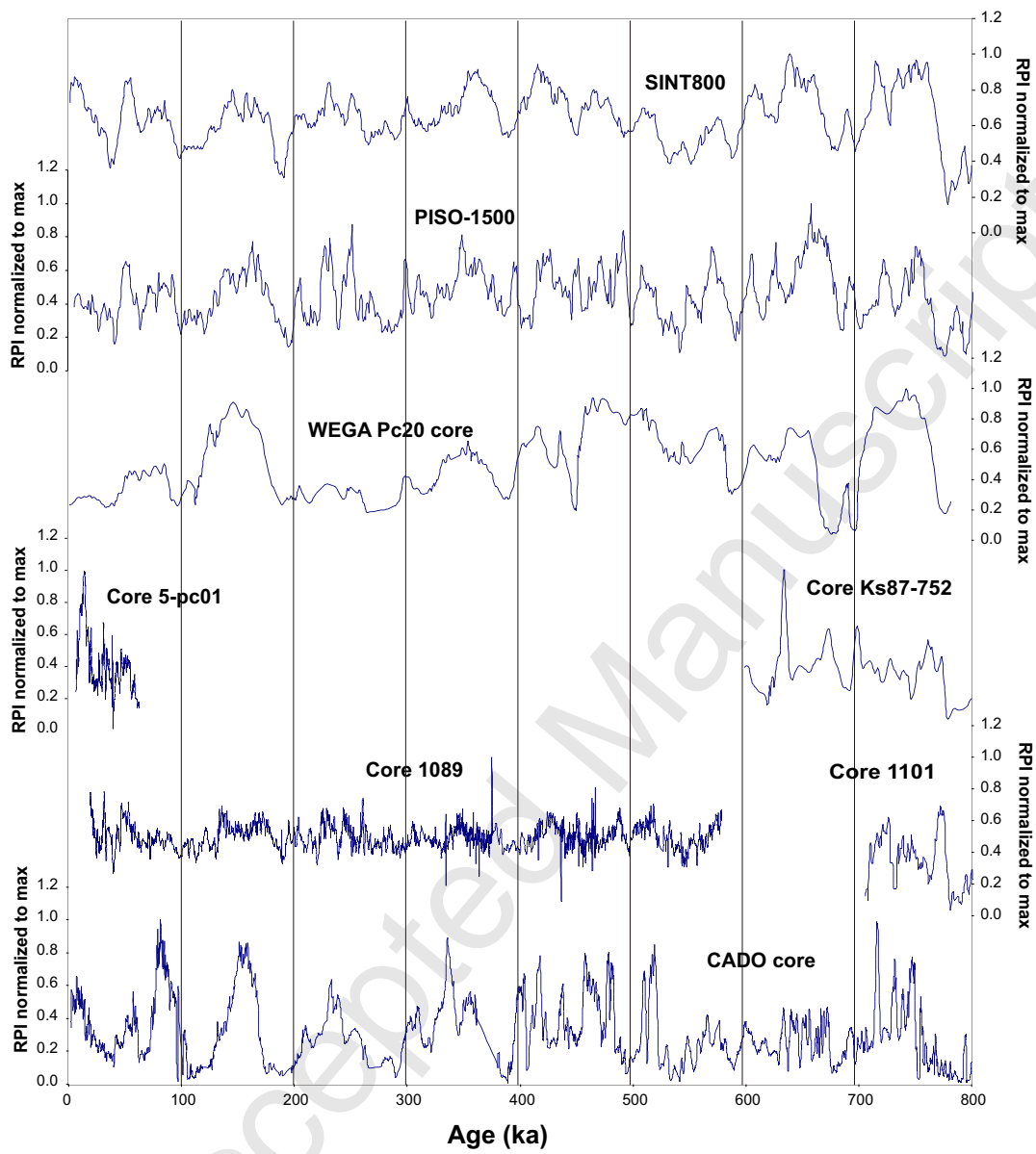


Fig. 8

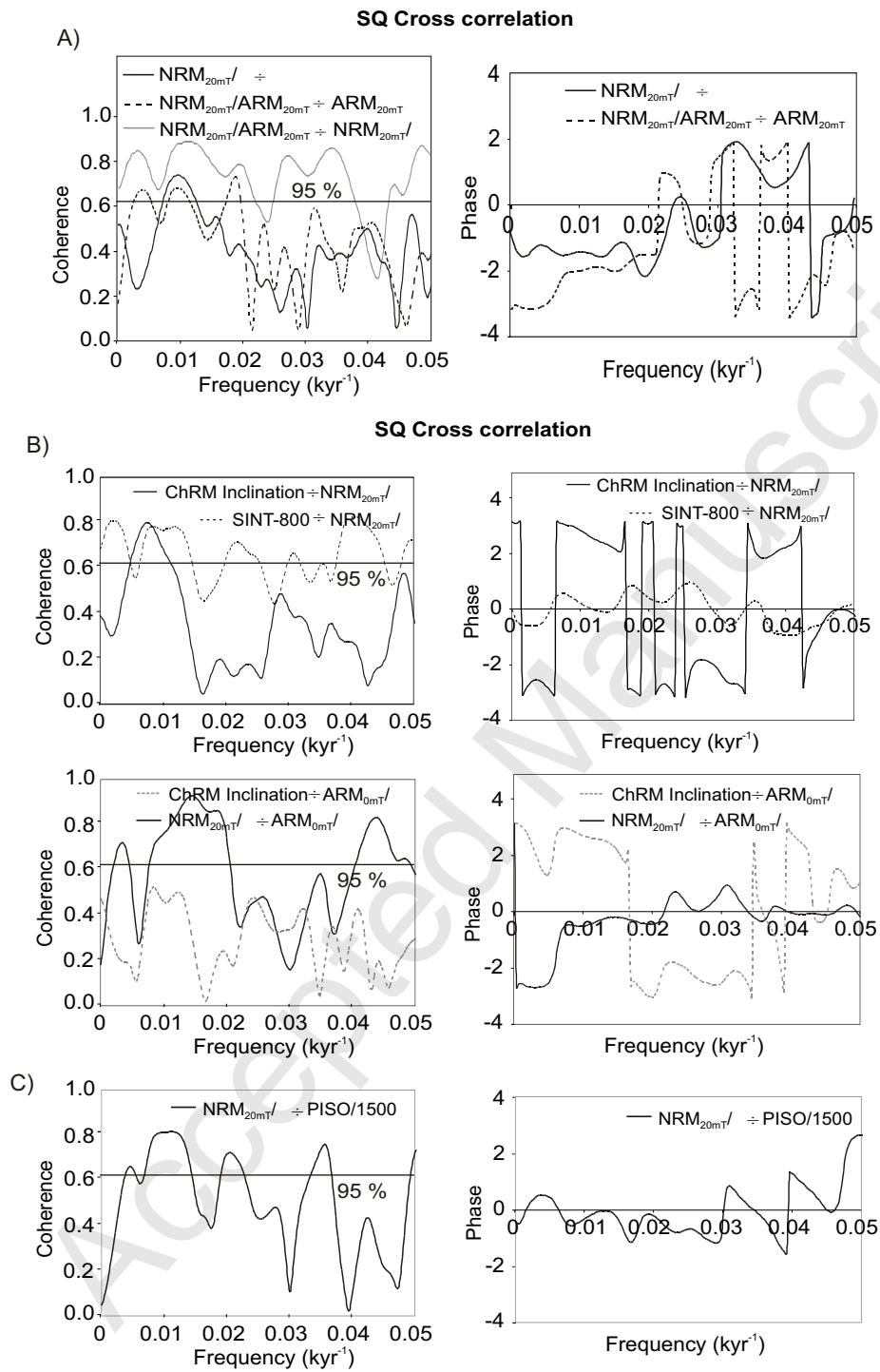


Fig.9



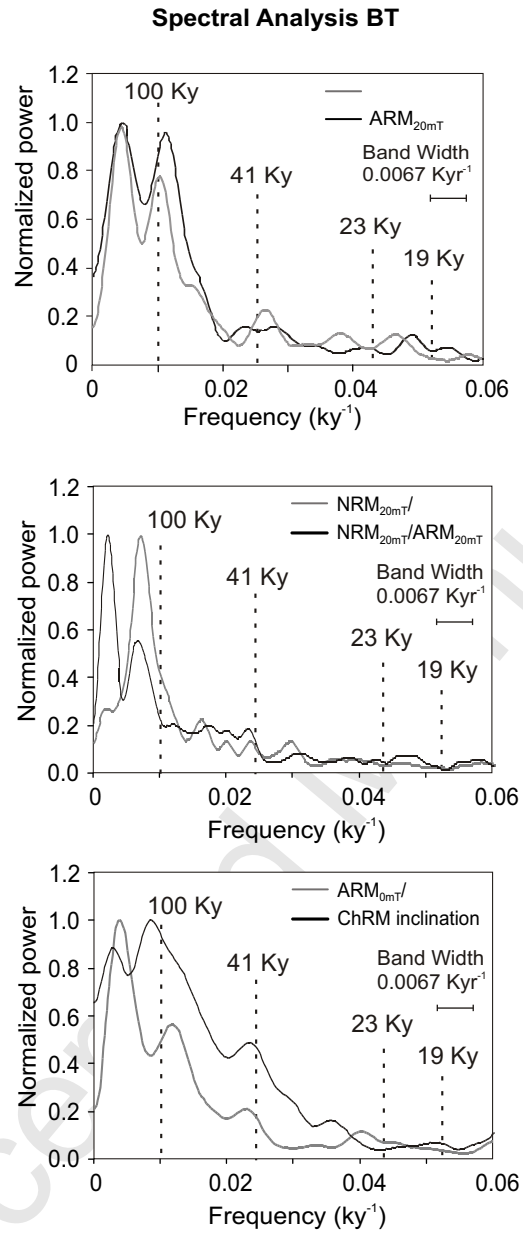
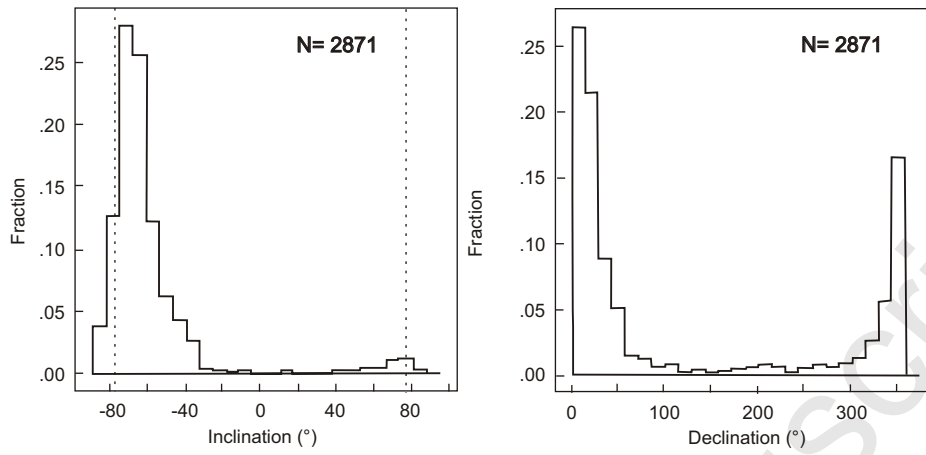


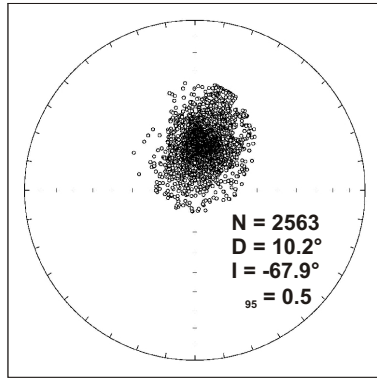
Fig. 10

A)



B)

Equal-area plot (normal)



Equal-area plot (reverse)

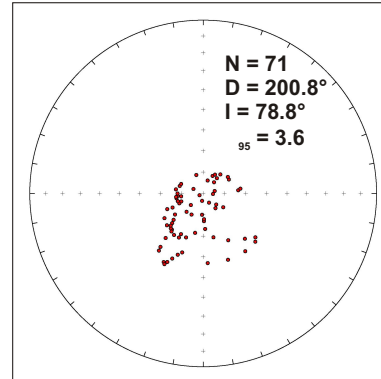
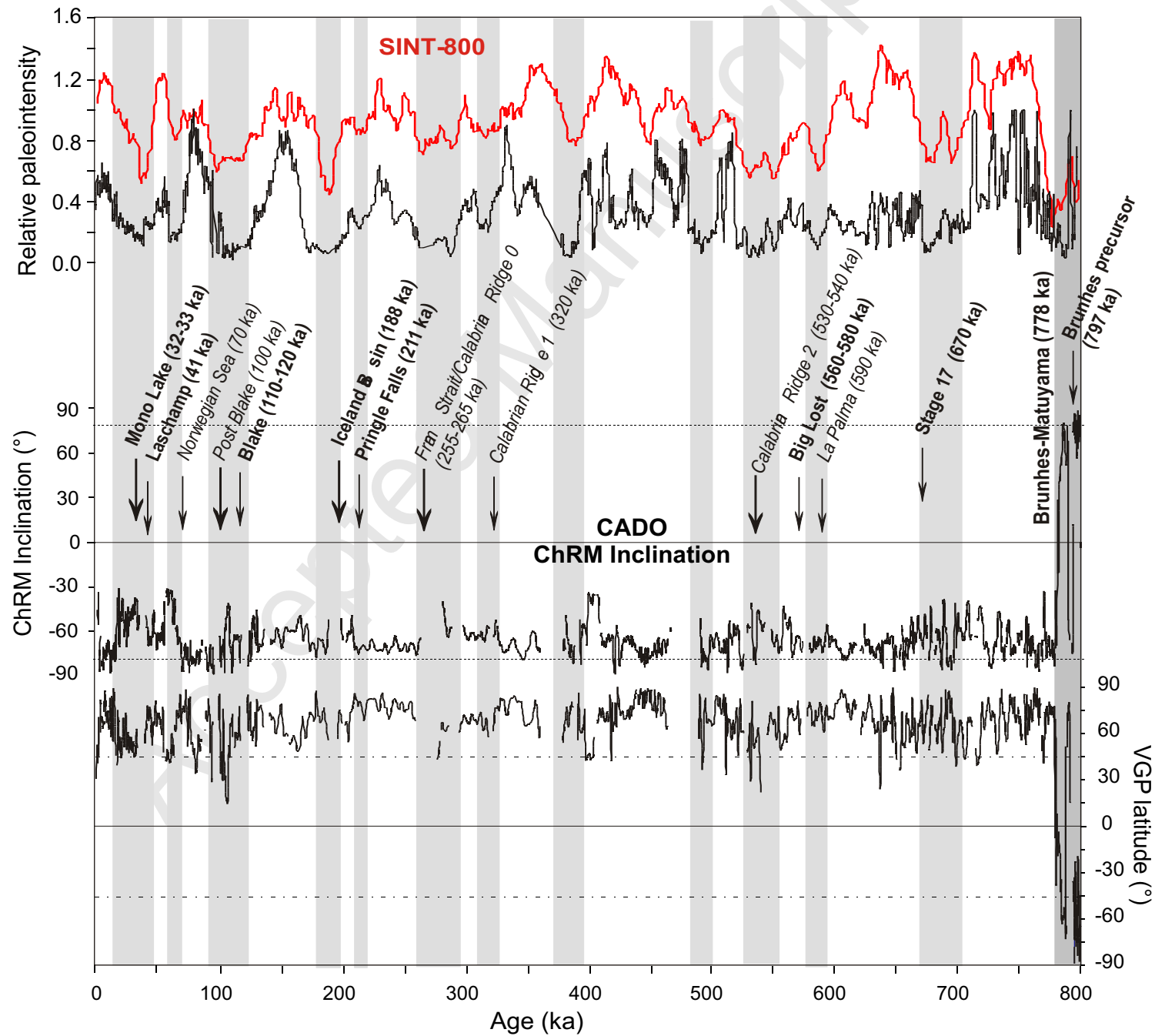


Fig.11



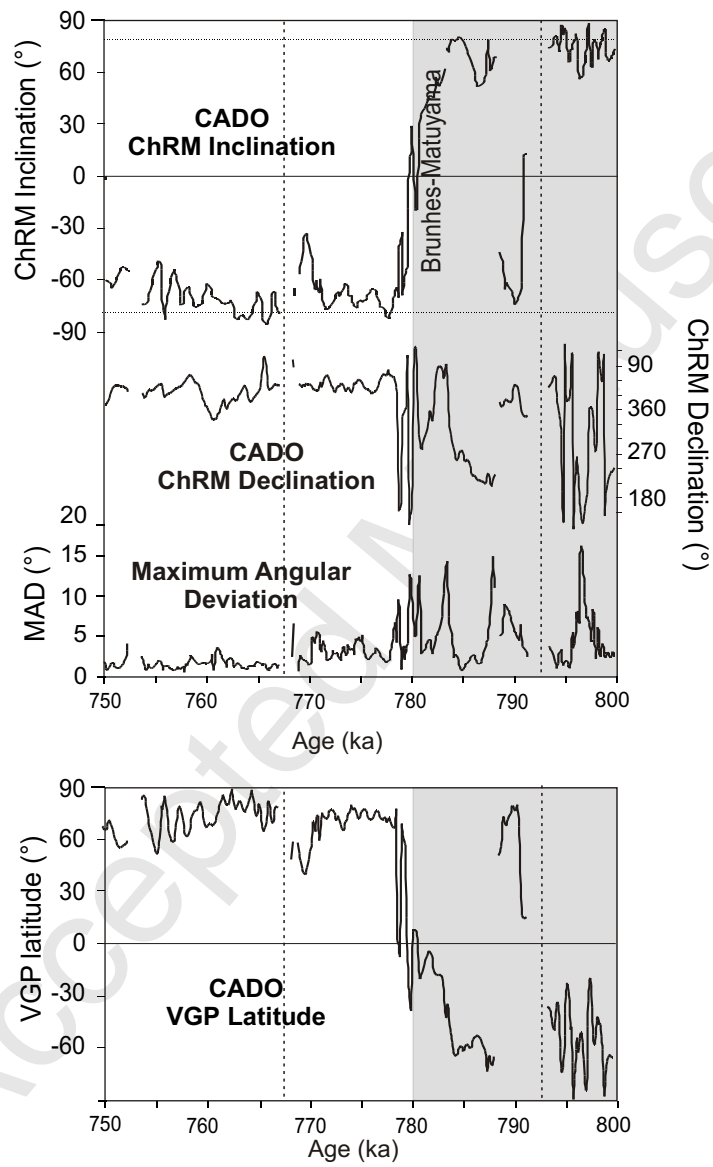


Fig.13